

A Rigorous Formalism of Unconventional Symmetry Breaking in Fermi Liquid Theory and Its Application to Nematicity in FeSe

Rina Tazai, Shun Matsubara, Youichi Yamakawa, Seiichiro Onari, and Hiroshi Kontani
Department of Physics, Nagoya University, Furo-cho, Nagoya 464-8602, Japan.

(Dated: February 3, 2023)

Unconventional symmetry breaking due to nonlocal order parameters has attracted considerable attention in many strongly correlated metals. Famous examples are the nematic order in Fe-based superconductors and the star-of-David charge density order in kagome metals. Such exotic symmetry breaking in metals is a central issue of modern condensed matter physics, while its theoretical foundation is still unclear in comparison with the well-established theory of superconductivity. To overcome this difficulty, here we introduce the “form factor” that generalizes the nonlocal order parameter into the Luttinger-Ward (LW) Fermi liquid theory. We then construct a rigorous formalism of the “density-wave equation” that gives the thermodynamically stable form factor, similarly to the superconducting-gap equation. In addition, a rigorous expression of the Ginzburg-Landau free-energy for the unconventional order is presented to calculate various thermodynamic properties. In the next stage, we apply the derived formalism to a typical Fe-based superconductor FeSe, by using the one-loop LW function that represents the free-energy gain due to the interference among paramagnons. The following key experiments are naturally explained: (i) Lifshitz transition (=disappearance of an electron-pocket) due to the bond+orbital order below T_c . (ii) Curie-Weiss behavior of the nematic susceptibility at higher T , and the deviation from the Curie-Weiss behavior at lower T near the nematic quantum-critical-point. (iii) Scaling relation of the specific heat jump at T_c , $\Delta C/T_c \propto T_c^b$ with $b \sim 3$. (Note that $b = 0$ in the BCS theory.) These results lead to a conclusion that the nematicity in FeSe is the bond+orbital order due to the “paramagnon interference mechanism”. The present theory paves the way for solving various unconventional phase transition systems.

I. INTRODUCTION

Recently, rich symmetry breaking phenomena due to unconventional order parameters have attracted considerable attention in various electron systems. Famous examples are the C_2 -symmetric nematic order in various Fe-based superconductors [1–4]. It has been established that the nematic state is driven by the electron-correlation, thanks to the “electronic nematic susceptibility” measurements performed by the shear-modulus analysis [5–7], the Raman spectroscopy [8–10], and the elastoresistivity measurements [11–14]. Similar nematic orders are also observed in magic-angle-twisted-bilayer-graphene [15, 16], titanium pnictide oxide [17], and cuprate superconductors [18–21]. Also, correlation-driven density-wave (DW) with nonzero wavevector ($\mathbf{q} \neq \mathbf{0}$) has attracted increasing attention recently. Famous examples are the star-of-David DW state in kagome metal CsV_3Sb_5 [22–25] the CDW states in cuprate superconductors [20, 21, 26–30], and the multipole DW states in heavy fermion systems [31–33]. Furthermore, more exotic odd-parity DW orders that accompany the charge or spin loop current have been discovered in kagome metals [34, 35], iridates [36], and cuprates [37].

We call these DW states “unconventional” because they have non-local and non- s -wave order parameters, in analogy to unconventional (non- s -wave) superconductivity. For example, the order parameter of the d -wave bond order is $O_{i,j} = \bar{O}(\delta_{|x-x'|,1}\delta_{|y-y'|,0} - \delta_{x-x',0}\delta_{|y-y'|,1})$, where (x, y) and (x', y') are the integer coordinates of i and j sites [20, 21, 26, 38–41]. (In high contrast, the

conventional magnetic order $m_i = n_{i\uparrow} - n_{i\downarrow}$ is local.) However, simple local spin-density-wave (SDW) is inevitably derived within the mean-field-level approximations for the Hubbard models with screened Coulomb interactions [42, 43]. Therefore, beyond-mean-field many-electron theories are necessary to understand the unconventional DW states. This is a difficult but very interesting theoretical problem, and this is a central issue of modern condensed matter physics. On the other hand, these unconventional DW states we are interested in are metallic, so the itinerant picture will be fruitful. In addition, the $U(1)$ gauge symmetry is preserved. Thus, it is promising to construct the formalism of the DW states on the basis of the microscopic Fermi liquid theory [44–47].

In general, the DW state at wavevector \mathbf{q} originates from the particle-hole (p-h) pairing condensation, $D_{\mathbf{k}}^{q\sigma} = (1 - P_0)\langle c_{\mathbf{k}+\mathbf{q},\sigma}^\dagger c_{\mathbf{k},\sigma} \rangle$, where $c_{\mathbf{k},\sigma}$ is the electron annihilation operator, \mathbf{k} is the momentum, and $\sigma (= \pm 1)$ is the spin index [38, 42, 43]. P_0 represents the projection onto the totally-symmetric state with respect to the space-group and the time-reversal [42, 43]. Rich classes of the DW states are determined by the symmetry of the p-h condensation $D_{\mathbf{k}}^{q\sigma}$. For example, a simple spin-DW state is given as the \mathbf{k} -independent function $D_{\mathbf{k}}^{q\sigma} = m\sigma$. The realized DW state $D_{\mathbf{k}}^{q\sigma}$ should be uniquely determined as the extremum of the free energy.

In Fermi liquids, the single-electron kinetic term between sites i and j is given by $t_{i,j}^\sigma = t_{i-j}^0 + \Sigma_{i,j}^\sigma$, where t_{i-j}^0 is the hopping integral of the bare Hamiltonian, and $\Sigma_{i,j}^\sigma$ is the self-energy due to the correlation between other electrons. Here, we define the symmetry breaking part

of the self-energy [42, 43]:

$$\delta t_{i,j}^\sigma \equiv (1 - P_0)\Sigma_{i,j}^\sigma. \quad (1)$$

In the absence of the DW order ($T \geq T_c$), we obtain $\delta t_{i,j}^\sigma = 0$ by definition. When the DW order emerges ($T \leq T_c$), $\delta t_{i,j}^\sigma$ becomes finite due to nonzero $D_{\mathbf{k}}^{q\sigma}$. Thus, $\delta t_{i,j}^\sigma$ is the energy-dimension order parameter of the DW state.

Here, we consider the DW state at a constant wavevector \mathbf{q} . For convenience, we introduce the ‘‘form factor $\delta t_{\mathbf{k}}^{q\sigma}$ ’’ that is the Fourier transform of $\delta t_{i,j}^\sigma$ [42, 43]:

$$\delta t_{\mathbf{k}}^{q\sigma} \equiv \frac{1}{N} \sum_{ij} \delta t_{ij}^\sigma e^{-i\mathbf{k}\cdot(\mathbf{r}_i - \mathbf{r}_j)} e^{-i\mathbf{q}\cdot\mathbf{r}_i}, \quad (2)$$

where \mathbf{r}_i is the position of site i . The classification of the symmetry of the form factor is presented in Sect. IA.

The theoretical way to derive the form factor $\delta t_{\mathbf{k}}^{q\sigma}$ has not been established yet. The aim of the present study is to establish an exact framework to derive $\delta t_{\mathbf{k}}^{q\sigma}$, based on which we can construct reliable and useful approximate theories. In the statistical mechanics, the symmetry breaking with $\delta t_{\mathbf{k}}^{q\sigma}$ occurs when the grand potential Ω is reduced. In other words, $\delta t_{\mathbf{k}}^{q\sigma}$ is uniquely determined as the stationary state with the minimum grand potential. In strongly correlated Fermi liquids, a rigorous formalism of the grand potential Ω is given by the Luttinger-Ward (LW) theory [45]. In the LW theory, the LW function $\Phi[G]$, which is the functional of electron Green function G , plays a central role. The self-energy Σ and the irreducible two-particle interaction I are uniquely derived from the functional derivatives of $\Phi[G]$ [45].

In this paper, we first introduced the ‘‘form factor $\delta t_{\mathbf{k}}^{q\sigma}$ ’’ into the LW theory to analyze the symmetry breaking at wavevector \mathbf{q} . Its $(\mathbf{k} - \mathbf{q}/2)$ -dependence represents the symmetry of the DW. We next derived the ‘‘DW equation’’ to obtain the form factor that minimize the LW ground potential below T_c . In this theory, the optimized $\delta t_{\mathbf{k}}^{q\sigma}$ is uniquely obtained because the DW equation is equivalent to the thermodynamic stationary condition. This formalism enables us to study rich variety of electron-correlation-driven DW states ($\delta t_{\mathbf{k}}^{q\sigma}$) without assuming any symmetry, like the analysis of the superconducting (SC) states ($\Delta_{\mathbf{k}}^{\sigma\sigma'}$) based on the SC gap equation. In addition, we derive an exact expression of the Ginzburg-Landau (GL) free energy, $F \propto a_{\mathbf{q}}\phi^2$, where ϕ is the amplitude of the DW order. The coefficient $a_{\mathbf{q}}$ is uniquely related to the eigenvalue of the DW equation $\lambda_{\mathbf{q}}$. Thus, we can calculate the thermodynamic properties and the stability of the DW state.

In the next stage, we apply the derived DW equation to FeSe by using the one-loop LW function $\Phi_{\text{FLEX}}[G]$ that represents the quantum interference among paramagnons. This theory naturally explains the following essential experimental reports: **(i)** Nematic Fermi surface (FS) and the Lifshitz transition due to bond+orbital order [48–51]. **(ii)** Curie-Weiss (CW) behavior of the nematic susceptibility χ_{nem} at higher temperatures, and

the deviation from the CW behavior at lower temperatures near the nematic quantum-critical-point (QCP). [12–14, 52]. **(iii)** Scaling relation of the specific heat jump at T_c , $\Delta C/T_c \propto T_c^b$ ($b \sim 3$). This relation naturally explains the smallness of (or undetected) $\Delta C/T_c$ reported in several nematic systems, such as RbFe_2As_2 ($T_c \sim 40\text{K}$) [53] and cuprate superconductors ($T_c \sim 200\text{K}$) [18, 19]. In cuprates, the nematic transition occurs at the pseudogap temperature T^* [18, 19], while no anomaly in specific heat at $T = T^*$ has been reported previously.

Interestingly, recent experiments have revealed that the nematic QCP is clearly separated from the magnetic QCP in $\text{Fe}(\text{Se},\text{S})$ and $\text{Fe}(\text{Se},\text{Te})$ [54] in addition to $\text{Na}(\text{Fe},\text{Co})\text{As}$ [55]. Such clear separation between two QCPs in addition to the key points **(i)**–**(iii)** are naturally understood by the present theory. Therefore, the nematicity in FeSe is the bond+orbital order due to the ‘‘paramagnon interference mechanism’’ [2, 3, 42, 56].

Here, we construct the DW equation based on the LW theory. The LW theory is expected to be valid for various strongly-correlated metals except for the vicinity of the localized Mott states. Thus, the present theory is expected to pave the path to understanding the useful concept of the ‘‘vestigial nematic order’’ from the itinerant picture.

A. Form Factor

Here, we discuss the rich variety of unconventional DW states [38, 42, 43, 57, 58] by classifying the symmetry of the form factor. The exotic DW states are represented by the non-local order parameter δt_{ij}^σ , which is parameterized by different site indices i and j . Then, the effective hopping integral is $t_{i,j}^\sigma = t_{i-j}^0 + \delta t_{ij}^\sigma$, where t_{i-j}^0 is the original hopping integral with A_{1g} symmetry. In conventional charge (spin) orders, the order parameter is expressed as $\delta t_{ij}^\uparrow = +(-)\delta t_{ij}^\downarrow$ with $i = j$, respectively.

In recent years, in contrast, unconventional non-local orders given by δt_{ij}^σ with $i \neq j$ have been discovered and attracted increasing attentions. Here, we assume the Hermitian order parameter [42, 43]:

$$\delta t_{ij}^\sigma = (\delta t_{ji}^\sigma)^*, \quad (3)$$

$$\delta t_{\mathbf{k}}^{q\sigma} = (\delta t_{\mathbf{k}+\mathbf{q}}^{-q\sigma})^*, \quad (4)$$

δt_{ij}^σ is classified into four channels in terms of parity symmetry ($\mathcal{P} = \pm 1$) and time-reversal symmetry ($\mathcal{T} = \pm 1$) as shown in Fig.1 (a). Below, we discuss the case of $\mathbf{q} = \mathbf{0}$. First, we consider the case of $\delta t_{ij}^\uparrow = \delta t_{ij}^\downarrow$. When δt_{ij} is real, the bond order with $(\mathcal{P}, \mathcal{T}) = (+1, +1)$ is realized. As an example, the d -wave bond order in square lattice model is shown in Fig. 1 (b). When δt_{ij} is pure imaginary, the charge-loop current (cLC) with $(\mathcal{P}, \mathcal{T}) = (-1, -1)$ is realized. Its form factor in \mathbf{k} -space is $\delta t_{\mathbf{k}} \propto \cos k_x - \cos k_y$. An example of the cLC order in anisotropic triangular lattice model is shown in Fig. 1 (c).

Next, we consider the case of $\delta t_{ij}^\uparrow = -\delta t_{ij}^\downarrow$. When δt_{ij} is real, the spin-bond order with $(\mathcal{P}, \mathcal{T}) = (+1, -1)$ appears. When δt_{ij} is pure imaginary, the spin-loop current (sLC) order with $(\mathcal{P}, \mathcal{T}) = (-1, +1)$ appears. An example of the sLC order is shown in Fig. 1 (d).

In addition, the translational symmetry is violated when the DW wavevector \mathbf{q} is nonzero. Furthermore, orbital orders [56], valley orders [16], and multipole orders [31] emerge when the Wannier functions possess multiple degrees of freedom. These rich non-local DW states are called the quantum-liquid-crystal (QLC) order [42], We note that, in a simple single-site model, the cLC and sLC orders in real space ($\delta t_{ij}^\sigma = -\delta t_{ij}^{\sigma'}$) are pure imaginary according to the Hermitian condition. However, the Fourier transformation of such current order $\delta t_{\mathbf{k}}^{\mathbf{q}\sigma}$ becomes real.

B. Stoner Theory for Ferro-Magnetic Transition

Here, we briefly review the mean-field theory of the ferro-magnetic (FM) transition and derive a simplified DW equation and GL free energy. This explanation will be useful to understand the derivation of the DW equation based on the LW theory in later sections. It is also understood that the mean-field theory is insufficient to explain the nematic order. Below, we consider the following Hubbard model,

$$H = \sum_{i \neq j, \sigma} t_{i-j}^0 c_{i\sigma}^\dagger c_{j\sigma} + H_I, \quad (5)$$

$$H_I = \sum_{i\sigma} U c_{i\sigma}^\dagger c_{i\sigma} c_{i\bar{\sigma}}^\dagger c_{i\bar{\sigma}} = \frac{U}{4} \sum_i (n_i^2 - m_i^2), \quad (6)$$

where $n_i = n_{i\uparrow} + n_{i\downarrow}$ and $m_i = n_{i\uparrow} - n_{i\downarrow}$. The conduction electron energy is $\epsilon_{\mathbf{k}} = \frac{1}{N} \sum_{i,j} t_{i-j}^0 e^{i(\mathbf{r}_i - \mathbf{r}_j) \cdot \mathbf{k}}$. In the mean-field approximation, the magnetic order is expressed as the spin-dependent δt : $\delta t_{ii}^\uparrow = -\delta t_{ii}^\downarrow = -\frac{U}{2} m_i$. Here, we set $M_i \equiv U m_i / 2$. In the case of the FM ($q = 0$) order, $M_i = M$. Thus, the grand potential is given by

$$\begin{aligned} \Omega_{\text{MF}} &= \frac{T}{N} \sum_{k, \sigma} \ln G_{k\sigma}^{\text{MF}} + \frac{1}{U} M^2 \\ &= -\frac{1}{N} \sum_{k, \sigma} \ln(1 + e^{-\beta(\epsilon_{k\sigma} - \mu)}) + \frac{1}{U} M^2, \end{aligned} \quad (7)$$

where $k \equiv (\mathbf{k}, \epsilon_n = (2n+1)\pi T)$, $\epsilon_{k\sigma} = \epsilon_{\mathbf{k}} + M\sigma$, and $G_{k\sigma}^{\text{MF}} = (i\epsilon_n - \epsilon_{k\sigma} + \mu)^{-1}$ is the electron Green function. From the stationary condition of the Ω_{MF} , which is given by $\partial\Omega_{\text{MF}}/\partial M = 0$, the mean-field equation for M is obtained as

$$M = -\frac{U}{2N} \sum_{k\sigma} f(\epsilon_{k\sigma})\sigma. \quad (8)$$

Next, we derive the linearized mean-field equation by linearizing the right-hand side of Eq. (8). It is given as

$$\alpha_S M = \frac{U}{N} \sum_{\mathbf{k}} \left(-\frac{\partial n(\epsilon_{\mathbf{k}})}{\partial \epsilon_{\mathbf{k}}} \right) M = U \chi^0(q=0) M, \quad (9)$$

where α_S is the eigenvalue, which reaches unity at the critical temperature. $n(\epsilon)$ is the Fermi distribution function. In the mean-field approximation, $\alpha_S = U \chi^0(0)$, where $\chi^0(0)$ is the irreducible susceptibility at $\mathbf{q} = 0$. α_S is called the spin Stoner factor. Equation (9) is the simplest example of the spin-channel DW equation with $I_{kk',q}^s = U$.

Here, we consider the GL free energy for the magnetic transition:

$$F_{\text{GL}} = aM^2 + \frac{1}{2}bM^4. \quad (10)$$

Here, $F_{\text{GL}} = \Omega_{\text{MF}} + \mu N$, where μ is the chemical potential. Based on Eq. (7), the coefficient a is expressed as

$$a = \chi^0(0) \left(-1 + \frac{1}{\alpha_S} \right). \quad (11)$$

This equation is consistent with the Stoner theory [60].

For the magnetic state at finite wavevector \mathbf{q} , the eigenvalue of Eq. (9) is given as $\alpha_S(\mathbf{q}) = U \chi^0(\mathbf{q}, 0)$, and the \mathbf{q} -dependent coefficient of the GL free energy becomes $a_{\mathbf{q}} = \chi^0(\mathbf{q}, 0) \left(-1 + \frac{1}{\alpha_S(\mathbf{q})} \right)$. Note that $a_{\mathbf{q}} \approx$

$$a_{\mathbf{q}=\mathbf{0}} + \frac{1}{2} \sum_{\mu}^{x,y,z} c_{\mu} q_{\mu}^2, \quad \text{where } c_{\mu} = \partial_{\mu}^2 a_{\mathbf{q}} / \partial q_{\mu}^2 |_{\mathbf{q}=\mathbf{0}}.$$

Here,

$$\chi^0(\mathbf{q}, 0) = \frac{1}{N} \sum_{\mathbf{k}} \frac{n(\epsilon_{\mathbf{k}+\mathbf{q}}) - n(\epsilon_{\mathbf{k}})}{\epsilon_{\mathbf{k}} - \epsilon_{\mathbf{k}+\mathbf{q}}}$$

is the irreducible susceptibility for general \mathbf{q} . The relation $\alpha_S > \alpha_S(\mathbf{q})$ holds for $\mathbf{q} \neq \mathbf{0}$ in ferromagnetic metals.

Considering the T -dependence of $\chi^0(0)$, the coefficient $a_{\mathbf{q}=\mathbf{0}}$ at $T = 0$ is given as

$$a_{\mathbf{q}=\mathbf{0}}(T=0) \simeq \frac{\pi^2}{3} B T_c^2, \quad (12)$$

where $B \equiv D''(0) + (D'(0))^2/D(0)$, and $D(0)$ is the density of states at the Fermi energy. Thus, the necessary condition for the FM transition ($T_c > 0$) is given as $B < 0$ in the mean-field approximation.

However, recent experiments have revealed that the ferro-DW order appears even in the case of $B > 0$ in several strongly correlated electron systems such as Fe-based superconductors. Thus, to understand the ferro-DW transition, we have to go beyond the mean field theory. In addition, exotic nonlocal DW orders (δt_{ij}^σ with $i \neq j$) summarized in Fig. 1 cannot be explained within the mean-field approximation. To solve these difficulties, in this paper, we study the DW phase transition on the bases of the LW theory.

II. DERIVATION OF DW-EQUATION FROM LUTTINGER-WARD THEORY

The Luttinger-Ward (LW) theory in Ref. [45] provides an exact expression of the grand potential Ω , which is applicable for strongly correlated metals unless the perturbation treatment is violated. In the first half part of this

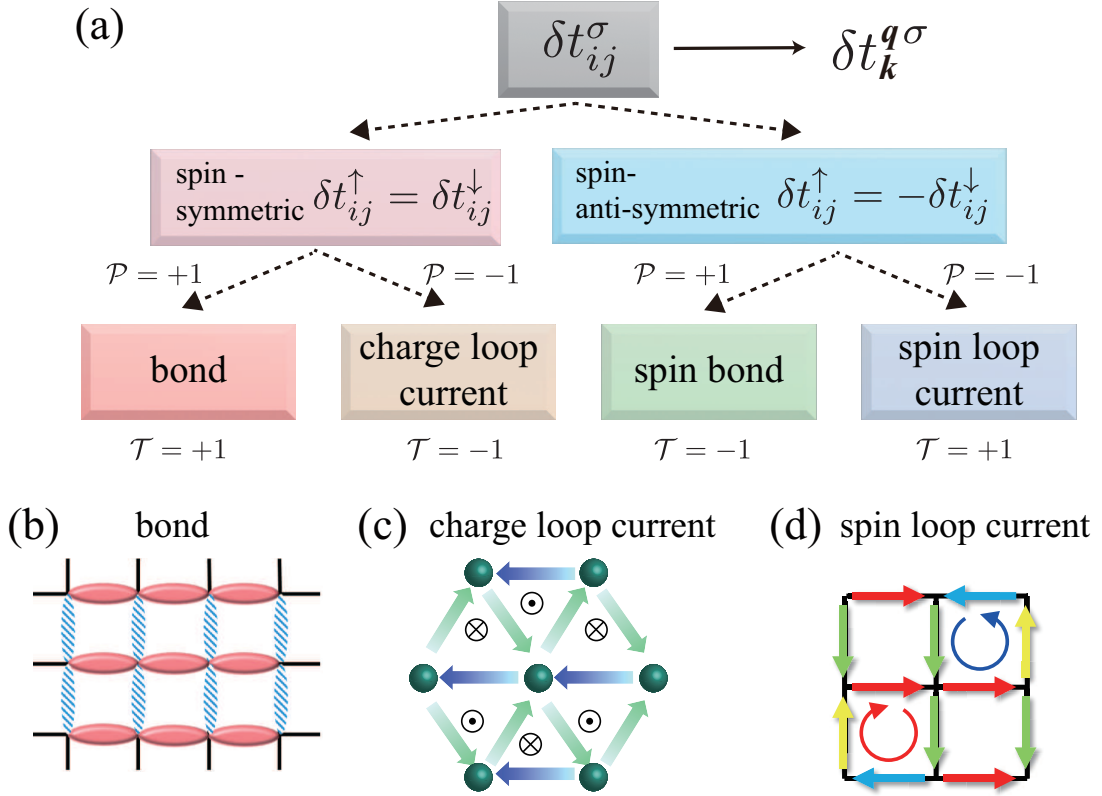


FIG. 1: (a) Classification of nonlocal order parameters (quantum liquid crystal states). Spin-symmetric (-antisymmetric) order corresponds to the charge (spin) channel order. The four states are labeled as $(\mathcal{P}, \mathcal{T})$, where $\mathcal{P} = \pm 1$ ($\mathcal{T} = \pm 1$) is the parity of the inversion-symmetry (time-reversal-symmetry). (b) d -wave bond order with $(\mathcal{P}, \mathcal{T}) = (+1, +1)$. (c) Charge-loop-current (cLC) order with $(\mathcal{P}, \mathcal{T}) = (-1, -1)$ in Ref. [59]. (d) Spin-loop-current (sLC) order with $(\mathcal{P}, \mathcal{T}) = (-1, +1)$ in Ref. [43].

section, we discuss the order parameter at $\mathbf{q} = \mathbf{0}$. Hereafter, we omit the orbital indices of the Green functions and the Coulomb interactions to simplify the expressions, because it is straightforward to denote them explicitly. In the LW theory, the grand potential is expressed as

$$\Omega_{\text{LW}}[G] = \Omega_{\text{F}}[G] + \Phi[G], \quad (13)$$

$$\Omega_{\text{F}}[G] = \frac{T}{N} \sum_{k\sigma} \left\{ \ln(G_{k\sigma}) - G_{k\sigma} \left((G_{k\sigma}^{\text{free}})^{-1} - G_{k\sigma}^{-1} \right) \right\}, \quad (14)$$

where $k \equiv (\mathbf{k}, \epsilon_n)$: $\mathbf{k} = (k_x, k_y)$ is the wavevector and $\epsilon_n = (2n + 1)\pi T$ is the fermion Matsubara frequency. Here, $T \sum_k \dots \equiv T \sum_{\epsilon_n} \sum_{\mathbf{k}} \dots$, and $G_{k\sigma}$ is the Green function with the self-energy: $G_{k\sigma} = \left((G_{k\sigma}^{\text{free}})^{-1} - \Sigma_{k\sigma} \right)^{-1}$. Now, the self-energy can be divided into

$$\Sigma = \Sigma^0 + \delta t, \quad (15)$$

where Σ^0 is the “normal state self-energy” without any symmetry breaking, and δt is equal to the DW order parameter introduced in Sec.I. Here, Σ^0 belongs to A_{1g} symmetry, while δt belongs to non- A_{1g} symmetry. Thus, $\delta t = 0$ for $T > T_c$.

In Eq. (14), $\Phi[G]$ is the Luttinger-Ward function which is given by calculating the all closed linked skeleton diagrams. Based on Eq. (14), we can define Ω as a functional of Σ [61].

$$\Omega[\Sigma] = -\frac{T}{N} \sum_{k\sigma} \ln \left(- (G_{k\sigma}^{\text{free}})^{-1} + \Sigma_{k\sigma} \right) + P[\Sigma], \quad (16)$$

where $P[\Sigma]$ is considered as the Legendre-transformation of $\Phi[G]$ introduced by Potthoff [61].

$$P[\Sigma] \equiv -\frac{T}{N} \sum_{k\sigma} G_{k\sigma} \Sigma_{k\sigma} + \Phi[G]. \quad (17)$$

In deriving the GL free energy, we have to analyze $\Omega[\Sigma]$ in Eq. (16). Using the Luttinger-Ward function Φ and Potthoff function F [61], the self-energy and Green function are respectively expressed as

$$\frac{\delta \Phi[G]}{\delta G_{k\sigma}} = \Sigma_{k\sigma}[G], \quad (18)$$

$$\frac{\delta P[\Sigma]}{\delta \Sigma_{k\sigma}} = -G_{k\sigma}[\Sigma]. \quad (19)$$

Then, the functional derivations of $\Omega[G]$ and $\Omega[\Sigma]$ are

respectively given by

$$\frac{\delta\Omega[G]}{\delta G_{k\sigma}} = G_{k\sigma}^{-1} - (G_{k\sigma}^{\text{free}})^{-1} + \Sigma_{k\sigma}[G], \quad (20)$$

$$\frac{\delta\Omega[\Sigma]}{\delta \Sigma_{k\sigma}} = \frac{1}{(G_{k\sigma}^{\text{free}})^{-1} - \Sigma_{k\sigma}} - G_{k\sigma}[\Sigma]. \quad (21)$$

When Ω is stationary, the following Dyson equation is satisfied,

$$\Sigma_{k\sigma}[G] = (G_{k\sigma}^{\text{free}})^{-1} - G_{k\sigma}^{-1} \quad (\text{from Eq.(20)} = 0), \quad (22)$$

$$G_{k\sigma}[\Sigma] = \frac{1}{(G_{k\sigma}^{\text{free}})^{-1} - \Sigma_{k\sigma}} \quad (\text{from Eq.(21)} = 0). \quad (23)$$

Based on the Luttinger-Ward theory, the ferro ($q = 0$) DW transitions are naturally described by the self-consistent equation (We call this the DW equation).

Here, we introduce the irreducible 4-point vertex $I_{kk'}^{\sigma\sigma'}$ shown in Fig.2 (a). It is a Jacobian connecting Σ and G as [61]

$$\frac{\delta \Sigma_{k\sigma}[G]}{\delta G_{k'\sigma'}} = I_{kk'}^{\sigma\sigma'}, \quad (24)$$

$$\frac{\delta G_{k\sigma}[\Sigma]}{\delta \Sigma_{k'\sigma'}} = \left\{ I_{kk'}^{\sigma\sigma'} \right\}^{-1}. \quad (25)$$

Therefore, the following analytical relation [61] is obtained:

$$\frac{T}{N} \sum_{k''\sigma''} \frac{\delta \Sigma_{k\sigma}[G]}{\delta G_{k''\sigma''}} \frac{\delta G_{k''\sigma''}[\Sigma]}{\delta \Sigma_{k'\sigma'}} = \delta_{kk'} \delta_{\sigma\sigma'}, \quad (26)$$

which is exactly satisfied when G is uniquely determined from Σ via one-to-one correspondence.

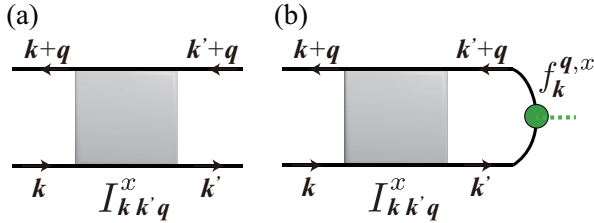


FIG. 2: (a) Definition of the irreducible 4-point vertex function I_{kkq}^x ($x = s, c$). (b) Right-hand side of the linearized DW equation composed of I_{kkq}^x . $f_k^{q,x}$ is the form factor at wavevector q .

The DW equation is derived from the following stationary conditions

$$\frac{\delta \Omega_{\text{LW}}[G]}{\delta \Sigma_{k\sigma}} \Big|_{\Sigma^0} = 0, \quad (\text{at any } T) \quad (27)$$

$$\frac{\delta \Omega_{\text{LW}}[G]}{\delta \Sigma_{k\sigma}} \Big|_{\bar{\Sigma}} = 0 \quad (T < T_c), \quad (28)$$

where Σ^0 is the self-energy without any symmetry breaking, and $\bar{\Sigma}$ is the stationary self-energy after the symmetry breaking. For $T > T_c$, the thermodynamic state is

given by Eq. (27), which corresponds to the minimum of the free energy shown in Fig. 3 (a). For $T < T_c$, Eq. (28) gives the symmetry breaking state shown in Fig. 3 (b). (Eq. (28) corresponds to the unstable extremum.)

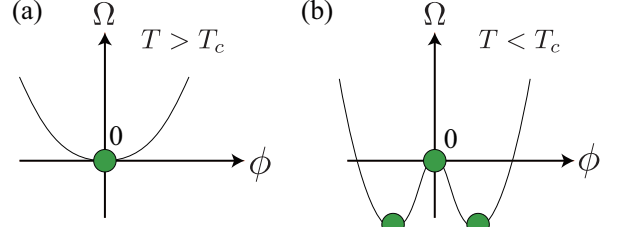


FIG. 3: Schematic picture of the GL free energy (a) above T_c ($a(T) > 0$) and (b) below T_c ($a(T) < 0$). Stationary points are shown by blue circles.

By using Eq.(28) and (21),

$$\begin{aligned} \frac{\delta \Omega_{\text{LW}}[G]}{\delta \Sigma_{k\sigma}} \Big|_{\bar{\Sigma}} &= -G_{k\sigma}^2 \Sigma_{k\sigma} + \frac{\delta \Phi[G]}{\delta \Sigma_{k\sigma}} \\ &= -G_{k\sigma}^2 \Sigma_{k\sigma} + \frac{T}{N} \sum_{k'\sigma'} \frac{\delta G_{k'\sigma'}}{\delta \Sigma_{k\sigma}} \frac{\delta \Phi[G]}{\delta G_{k'\sigma'}} \end{aligned} \quad (29)$$

where $\frac{\delta G_{k'\sigma'}}{\delta \Sigma_{k\sigma}} = G_{k\sigma}^2 \delta_{kk'}$. Thus, the stationary condition of Eq. (28) is rewritten as

$$\frac{\delta \Phi[G]}{\delta G_{k\sigma}} \Big|_{G^0} = \Sigma_{k\sigma}^0, \quad (30)$$

$$\frac{\delta \Phi[G]}{\delta G_{k\sigma}} \Big|_{\bar{G}} = \bar{\Sigma}_{k\sigma}, \quad (31)$$

where $\hat{G}^0 = (\{\hat{G}^{\text{free}}\}^{-1} - \hat{\Sigma}^0)^{-1}$. Equations (30) and (31) compose the ‘‘exact DW equation’’ that describes the DW state below T_c . Then, the order parameter is $\delta t_{k\sigma} = \bar{\Sigma}_{k\sigma} - \Sigma_{k\sigma}^0$.

It is noteworthy that superconducting gap equation is derived from the stationary condition of the LW function in the SC state $\delta \Phi[G, F]$, where F (G) is the anomalous (normal) Green function [62]. Thus, the derived DW equation for the form factor, Eqs. (30) and (31), is well-founded comparable with the well-known superconducting-gap equation.

Next, we derive the linearized DW equation with respect to δt . By subtracting Eq. (30) from (31), we obtain

$$\begin{aligned} \delta t_{k\sigma} &= \frac{T}{N} \sum_{k'\sigma'} \frac{\delta^2 \Phi[G]}{\delta G_{k'\sigma'} \delta G_{k\sigma}} \Big|_{\bar{G}} \delta G_{k'\sigma'} \\ &= \frac{T}{N} \sum_{k'\sigma'} \frac{\delta^2 \Phi[G]}{\delta G_{k'\sigma'} \delta G_{k\sigma}} \Big|_{G^0} \delta G_{k'\sigma'} + O(\delta G^2), \end{aligned} \quad (32)$$

where $\delta G \equiv \bar{G} - G^0$. Here, we rewrite $\delta t_{k\sigma}$ as

$$\delta t_{k\sigma} \equiv \phi \cdot f_{k\sigma}, \quad (33)$$

where ϕ is a real parameter, and f_k^q is the normalized order parameter that belongs to one of the irreducible representations in non- A_{1g} symmetry. It is convenient to set $\max_k |f_{k\sigma}| = 1$ because the relation $\phi = \max_k |\delta t_{k\sigma}|$ holds. Thus, we derive the following ‘‘linearize DW equation for $\mathbf{q} = \mathbf{0}$ ’’ by introducing the eigenvalue λ to the left-hand side of Eq. (32);

$$\lambda f_{k\sigma} = \frac{T}{N} \sum_{k'\sigma'} I_{kk'}^{\sigma\sigma'} (G_{k'\sigma'}^0)^2 f_{k'\sigma'}, \quad (34)$$

where we denote $I_{kk'}^{\sigma\sigma'} \equiv I_{kk'}^{\sigma\sigma'} \Big|_{\Sigma^0}$ to simplify the notation. In Eq. (34), the largest eigenvalue λ reaches unity at $T = T_c$, and its eigenvector gives the form factor of the DW state.

The linearized DW equation can be generalized for finite q orders as follows. First, we consider the DW order with the wavevector $\mathbf{q} = \mathbf{g} \cdot \mathbf{m}/n$ where \mathbf{g} is the reciprocal lattice vector, and m, n are integers ($0 \leq m < n$). Then, we can introduce the $n \times n$ -matrix Green function $G_k^{lm} = \langle k + lq | \hat{G} | k + mq \rangle$ where $l, m = 0 \sim n-1$. In this case, Eq. (31) becomes

$$\frac{\delta\Phi[G]}{\delta G_{k\sigma}} \Big|_{\bar{G}^{lm}} = \bar{\Sigma}_{k\sigma}^{lm}. \quad (35)$$

Hereafter, we drop the overlines of \bar{G} and $\bar{\Sigma}$ to simplify the notation.

Here, we adopt the extended Brillouin zone scheme for \vec{k} to simplify the explanation. After that, the DW equation can be linearized with respect to the \mathbf{q} -linear term in δt given by $\delta t^{m+1,m} \equiv \delta t_k^q$. By introducing the q -dependent eigenvalue, we obtain the following ‘‘linearize DW equation for general \mathbf{q} ’’,

$$\lambda_q f_{k\sigma}^q = \frac{T}{N} \sum_{k'\sigma'} I_{kk'}^{\sigma\sigma'} G_{k'\sigma'}^0 G_{k'+q\sigma'}^0 f_{k'\sigma'}^q, \quad (36)$$

where $q \equiv (\mathbf{q}, \omega_l)$: $\mathbf{q} = (q_x, q_y)$ is the wavevector and $\omega_l = 2l\pi T$ is the boson Matsubara frequency. The condition $\lambda_q = 1$ brings the DW transition temperature T_c with wavevector q , which can be interpreted as the particle-hole (p-h) gap equation. The form factor of the eigenvalue equation (36) contains the uncertainty of the phase factor $e^{i\theta}$. The correct phase θ is uniquely fixed by following the Hermitian condition in Eq. (4).

The DW equation (36) is further simplified by introducing the spin (s) and charge (c) channel functions in the absence of the spin-orbit interaction [43]:

$$f^{c(s)} = f_{\uparrow} + (-)f_{\downarrow}. \quad (37)$$

$$I^{c(s)} = I^{\uparrow\uparrow} + (-)I^{\uparrow\downarrow}. \quad (38)$$

Finally, we derive the simplified ‘‘linearized DW equation for x ($= s, c$) channel form factor at q ’’ from Eq. (36) as follows:

$$\lambda_q^x f_k^{q,x} = \frac{T}{N} \sum_{k'} I_{kk'}^x G_{k'}^0 G_{k'+q}^0 f_{k'}^{q,x}. \quad (39)$$

The right-hand side of Eq. (39) is shown in Fig.2 (b). Therefore, we derived the exact expression of the DW equation in Eq. (36) or Eq. (39) composed of the true irreducible four-point vertex I and the self-energy.

We can derive the expression of λ_q^x from Eq. (39) as

$$\lambda_q^x = X_q^x / \chi^{0f}(q), \quad (40)$$

where X is given as

$$X_q^x = \frac{T^2}{N^2} \sum_{k,k'} (f_k^{q,x})^* G_k^0 G_{k+q}^0 I_{kk'q}^x G_{k'}^0 G_{k'+q}^0 f_{k'}^{q,x}, \quad (41)$$

and $\chi^{0f}(q)$ is the irreducible susceptibility with the form factor $f_{k\sigma}^q$:

$$\chi^{0f}(q) \equiv -\frac{T}{N} \sum_{k\sigma} f_{k\sigma}^q G_{k+q\sigma}^0 G_{k\sigma}^0 f_{k\sigma}^{-q}. \quad (42)$$

From Eq. (40), the relation $\lambda_q^x \propto X_q^x$ is obtained because $\chi^{0f}(q)$ is nearly T -independent.

It is noteworthy that the DW equation introduced by Onari and Kontani *et al.* in Refs. [3, 20, 21, 42], which has been applied to iron-based and cuprate superconductors, is derived from the exact DW equation given in Eq. (36). The detailed derivation is shown in Appendix A.

Before closing this section, we reproduce the Stoner theory by applying the mean-field approximation to Eq. (39). In the mean-field theory,

$$I_{kk'q}^s = -U, \quad \delta\Sigma_k^{q,s} = M\delta_{q,0}. \quad (43)$$

Therefore, the Eq. (39) is given by

$$\lambda^s M = -\frac{T}{N} \sum_{k'} G_k^0 G_{k'}^0 U M = U \chi^0 M. \quad (44)$$

Thus, the eigenvalue for the ferromagnetic transition corresponds to the Stoner factor α_S :

$$\lambda^s = U \chi^0 \equiv \alpha_S. \quad (45)$$

III. DERIVATION OF GL FREE ENERGY BASED ON THE LINEARIZED DW EQUATION

A. GL free energy for DW state with form factor f

Here, we derive the expression of the Ginzburg-Landau (GL) free energy based on the DW-equation. The GL free energy due to the ferro-DW transition ($\delta t_{k\sigma} = \phi f_{k\sigma}$) is expressed as

$$\Omega_{\text{DW}}(T, \mu, \phi) = a(T)\phi^2 + \frac{1}{2}b\phi^4. \quad (46)$$

Its schematic picture above T_c ($a(T) > 0$) and that below T_c ($a(T) < 0$) are shown in Figs. 3 (a) and (b), respectively.

Note that the coefficients a and b are functional of the form factor $f_{k\sigma}$. By using the $\Omega[\Sigma]$ defined in Eq.(16), the coefficient a is calculated from the second functional derivation of $\Omega[\Sigma]$ as

$$\begin{aligned} \Omega[\Sigma^0 + \delta t] - \Omega[\Sigma^0] \\ \approx \frac{T}{N} \sum_{k\sigma k'\sigma'} \left. \frac{\delta^2 \Omega[\Sigma]}{\delta \Sigma_{k'\sigma'} \delta \Sigma_{k\sigma}} \right|_{\Sigma=\Sigma^0} \delta t_{k'\sigma'} \delta t_{k\sigma}. \end{aligned} \quad (47)$$

By using Eq. (21), we obtain

$$\begin{aligned} \frac{\delta^2 \Omega[\Sigma]}{\delta \Sigma_{k'\sigma'} \delta \Sigma_{k\sigma}} &= \frac{\delta}{\delta \Sigma_{k'\sigma'}} \left\{ \frac{1}{(G_{k\sigma}^{\text{free}})^{-1} - \Sigma_{k\sigma}} - G_{k\sigma}[\Sigma] \right\} \\ &= G_{k\sigma}^2 \delta_{kk'} - \frac{\delta G_{k\sigma}[\Sigma]}{\delta \Sigma_{k'\sigma'}} \\ &= (G_{k\sigma}^0)^2 \delta_{kk'} - \left\{ I_{kk'}^{\sigma\sigma'} \right\}^{-1}, \end{aligned} \quad (48)$$

where we used the relation in Eq. (25). Therefore, the Eq. (47) is rewritten as

$$\begin{aligned} \Omega[\Sigma^0 + \delta t] - \Omega[\Sigma^0] &\approx \frac{T}{N} \sum_{k\sigma} (G_{k\sigma}^0)^2 (\delta t_{k\sigma})^2 \\ &- \frac{T}{N} \sum_{k\sigma k'\sigma'} \left\{ I_{kk'}^{\sigma\sigma'} \right\}^{-1} \delta t_{k\sigma} \delta t_{k'\sigma'}. \end{aligned} \quad (49)$$

Here, we recall that the order parameter $\delta t_{k\sigma} = \phi \cdot f_{k\sigma}$ is determined by using the DW equation (36). By using Eq. (36) together with Eqs. (24)-(26), Eq. (49) is rewritten as

$$\begin{aligned} \Omega[\Sigma^0 + \delta t] - \Omega[\Sigma^0] &\simeq \left(1 - \frac{1}{\lambda}\right) \frac{T}{N} \sum_{k\sigma} (G_{k\sigma}^0)^2 f_{k\sigma}^2 \phi^2 \\ &= -2\chi^{0f}(0) \left\{1 - \frac{1}{\lambda}\right\} \phi^2, \end{aligned} \quad (50)$$

where the factor 2 originates from the spin degeneracy.

We can derive the GL free energy for the order parameter at nonzero wavevector q by considering the large unit cell as we discussed in Sect. II. Thus, the coefficient a defined in the Gibbs free energy in Eq. (46) is obtained as

$$a_q(T) = -2\chi^{0f}(q) \left(1 - \frac{1}{\lambda_q}\right). \quad (51)$$

As a result, we obtain the exact expression for coefficient a_q by using the eigenvalue λ_q in the DW equation. The obtained general expression in Eqs. (42) and (51) are meaningful to discuss the DW transition.

Finally, we stress that the Potthoff's Legendre-transformation of the LW formalism [61] is necessary to derive the correct GL free energy expression. In Appendix B, we explain that the expansion of (14) with respect to δt leads to an inaccurate expression.

B. GL free energy for BCS Superconductivity

Here, we consider the GL equation for the spin-singlet superconductivity. Here, we express the spin-singlet SC gap function as $\Delta_k = \psi \cdot f_k$, where f_k is the normalized form factor. Based on the LW theory for the superconducting states, we can derive that the second order GL parameter is given by

$$a(T) = -2\chi_{\text{pp}}^{0\psi}(0) \left(1 - \frac{1}{\lambda_{\text{sc}}}\right), \quad (52)$$

$$\chi_{\text{pp}}^{0\psi}(0) = \frac{T}{N} \sum_k |\psi_k|^2 G_k^0 G_{-k}^0, \quad (53)$$

where λ is the eigenvalue of the linearized gap equation given by

$$\lambda_{\text{sc}} f_k = \frac{T}{N} \sum_{k'} V_{kk'} G_{k'}^0 G_{-k'}^0 f_{k'}, \quad (54)$$

where $V_{kk'} = \left. \frac{\delta^2 \Phi}{\delta F \delta F^\dagger} \right|_{\Delta=0}$. Here, F and F^\dagger are anomalous Green functions. The derivation of Eq. (52) is essentially the same as that for the DW transition given in previous sections. We can show that the relationship (52) is also valid for the spin-triplet superconductivity.

IV. NUMERICAL ANALYSIS OF NEMATIC STATE IN FESE

In this section, we explain the important unsolved problems in FeSe, which is one of the most famous Fe-based superconductors. We try to understand the following key topic on the nematicity, for both above and below the nematic transition temperature T_c , based on a unified theory. **(i)** Lifshitz transition below T_c . **(ii)** Nematic susceptibility above and below T_c . **(iii)** Specific heat jump at $T = T_c$. In FeSe, T_c corresponds to the structure transition temperature T_S .

In previous sections, we derived the exact expressions of the linearized DW equation in Eq. (39) for $T > T_c$ and the full DW equation in Eqs. (30)-(31) for $T < T_c$. Here, we solve these equations for FeSe based on the one-loop approximation for the LW function, Φ_{FLEX} , derived in Appendix A. We include the normal state (=without order parameter) self-energy Σ^0 into the DW equations because it is necessary to satisfy the stationary condition (30)-(31), although it was dropped in previous studies [3].

We study a realistic $d+p$ orbital Hubbard model with on-site multiorbital Coulomb interaction U for FeSe:

$$H = H_0 + rH_U, \quad (55)$$

where H_0 is the $d+p$ orbital tight-binding model for FeSe, and H_U is the d -orbital Coulomb interaction for $d+p$ orbital model given by the constrained-random-phase-approximation (cRPA) method. The matrix elements in

H_U are composed of the intra-orbital Coulomb repulsion $U_{l,l}$, the inter-orbital Coulomb repulsion $U_{l,m}$ ($l \neq m$), and the exchange term $J_{l,m}$, as we explain in Appendix C.

In Eq. (55), $r (< 1)$ is the reduction factor of H_U that represents the screening due to p orbitals. According to Ref. [63], the averaged intra-orbital $U_{av} \sim 7eV$ is reduced to $\sim 4eV$ due to the screening effect by p -orbitals. In the present study, we set $r = 0.3 \sim 0.4$, where T_c increases with r . In contrast, T_c slowly decreases with r for $r > 0.5$. Thus, obtained T_c depends on r , while the symmetry and the form factor of the nematic order is insensitive to the choice of r . We note that the relation $\alpha_S < 1$ is satisfied for any r in the present two-dimensional FeSe model because the FLEX approximation satisfies the Mermin-Wagner theorem [64]. This fact is favorable for realizing the nonmagnetic nematic state ($\lambda > 1$ and $\alpha_S < 1$).

In the present numerical study for FeSe, we use 64×64 \mathbf{k} -meshes, and 4096 or 8192 Matsubara frequencies. Figure 4 (a) represents the Fermi surface (FS) of FeSe model. We derive the normal self-energy Σ^0 by applying the FLEX approximation. In the case of $r = 0.36$, the obtained orbital-dependent mass-enhancement factors at $T = 10\text{meV}$ are about $z_{xy}^{-1} \sim 5$ and $z_{xz,yz}^{-1} \sim 3$, respectively. The Stoner factor is about 0.9 and its T -dependence is very weak.

A. Above T_c : linearized DW equation analysis

First, we analyze the multiorbital Hubbard model for FeSe based on the linearized DW equation in Eq. (39), with the kernel function in Eq. (A3). Here, we incorporate the normal state self-energy Σ^0 given in Eq. (A2) into the DW equation to perform the conserving approximation. Σ^0 is significant to derive realistic T_c and beautiful CW/non-CW behaviors of χ_{nem} , although it has been dropped in our previous analyses.

Here, we discuss the kernel function in Eq. (A3). The first line in Eq. (A3) gives the Hartree term, Maki-Thompson (MT) term, and the second and the third lines in Eq. (A3) give the Aslamazov-Larkin (AL) terms. Both MT and AL terms cause important ‘‘fluctuation-induced interaction for the DW’’. In Fe-based SCs, the nematic order mainly originates from the AL terms, which represent the ‘‘interference between paramagnons’’ [2, 3, 56, 65]. The MT term is also important to induce the characteristic sign-reversing in the form factor in \mathbf{k} -space [1, 3]. On the other hand, the cLC orders in geometrically frustrated Hubbard models mainly originate from the the MT terms [59]. Note that the MT terms induce striking non-Fermi-liquid transport phenomena near the QCPs [66].

Figure 4 (b) shows the \mathbf{q} -dependence of the largest charge-channel eigenvalue $\lambda_{\mathbf{q}}^c$ at $r = 0.40$ and $T = 5\text{meV}$ derived from the DW equation. (Below, we drop the superscript c of $\lambda_{\mathbf{q}}^c$ for simplicity.) The obtained $\lambda_{\mathbf{q}}$ exhibit the maximum at $\mathbf{q} = \mathbf{0}$ because the convolution of two

$\chi_{\mathbf{q}}^{s^s}$, $C_{\mathbf{q}} \equiv \sum_p \chi_p^s \chi_{p+\mathbf{q}}^s$, included in the AL-type VCs include is largest at $\mathbf{q} = \mathbf{0}$. Here, $\lambda_{\mathbf{q}=\mathbf{0}}$ exceeds unity, and typical transition temperature T_c ($\sim 100\text{K}$) in Fe-based SCs is reproduced by including Σ^0 . We note that similar results were obtained in Fig. S4 (a) in Ref. [67] by taking Σ^0 into account.

The obtained form factors belong to B_{1g} symmetry, which is shown in Fig.4 (c): The xz, yz -orbital form factors express the \mathbf{k} -dependent orbital polarization, which has been reported by previous DW equation studies without Σ^0 [3]. The obtained xz, yz -orbital polarization elongates the hole-pocket along the k_y -axis as experimentally reported in Refs. [48, 68]. In addition, the xy -orbital form factor represents the d -orbital bond order $f \propto \cos k_x - \cos k_y$ emerges at the same T_c . This d -wave order leads to the disappearance of an electron-pocket around Y-point [49–51]. Thus, experimentally-observed ferro-nematic order in FeSe is naturally obtained. We stress that the coexistence of the xz, yz -orbital order and the $d_{x^2-y^2}$ -wave bond order on xy -orbital was already reported in Fig. S3 (a)-(d) in Ref. [67]. In addition, the d_{xy} -wave bond order on xy -orbital has been studied in RbFe_2As_2 in Ref. [69].

We comment that a simple A_{1g} symmetry order that accompanies the net charge order is suppressed by the Hartree term in the kernel function. In contrast, the B_{1g} symmetry order in Fig. 4 (c) is free from the suppression by the Hartree term due to sign reversal in the form factor.

Figure 4 (d) shows the temperature-dependence of $\lambda_{\mathbf{q}=\mathbf{0}}(T)$ for $r = 0.40 \sim 0.32$. At higher temperatures ($T \gtrsim 10\text{meV}$), $\lambda_{\mathbf{q}=\mathbf{0}}(T)$ exhibits the T -linear behavior. The nematic susceptibility above T_c is $\chi_{\text{nem}} = \chi^{0f}(0)(1 - \lambda_{\mathbf{q}=\mathbf{0}})^{-1}$, as proved theoretically in Ref. [69]. Therefore, it is confirmed that the experimental CW behavior of χ_{nem} at higher temperature is naturally explained in the present theory. The deviation from the CW behavior at lower temperatures will be discussed in Sect. VB.

Figure 4 (e) shows the obtained $R = (-\dot{\lambda}T_c)$ as a function of T_c . Here, $\dot{\lambda} \equiv \left. \frac{d\lambda}{dT} \right|_{T_c}$, R approximately corresponds to $\lambda_{\mathbf{q}=\mathbf{0}}(T = 0) - 1$, and R becomes very small when $T_c \ll 10\text{meV}$. The reason is the recovery of the Fermi-liquid behavior $\lambda(0) - \lambda(T) \propto T^2$ because the system is far from the magnetic QCP. Also, the relation $R \propto T_c^b$ ($b \sim 3$) is satisfied in the present study. In Sect. VA, we will explain that R is proportional to the jump in the heat capacity at T_c .

B. Below T_c : full DW equation analysis

Next, we analyze the full DW equation given as Eqs. (30)-(31) for $T < T_c$. We safely assume the uniform ($\mathbf{q} = \mathbf{0}$) order parameter because $\lambda_{\mathbf{q}}$ takes the largest value at $\mathbf{q} = \mathbf{0}$ as found in Fig. 4 (b). The aim of this subsection is to explain the essential properties of the

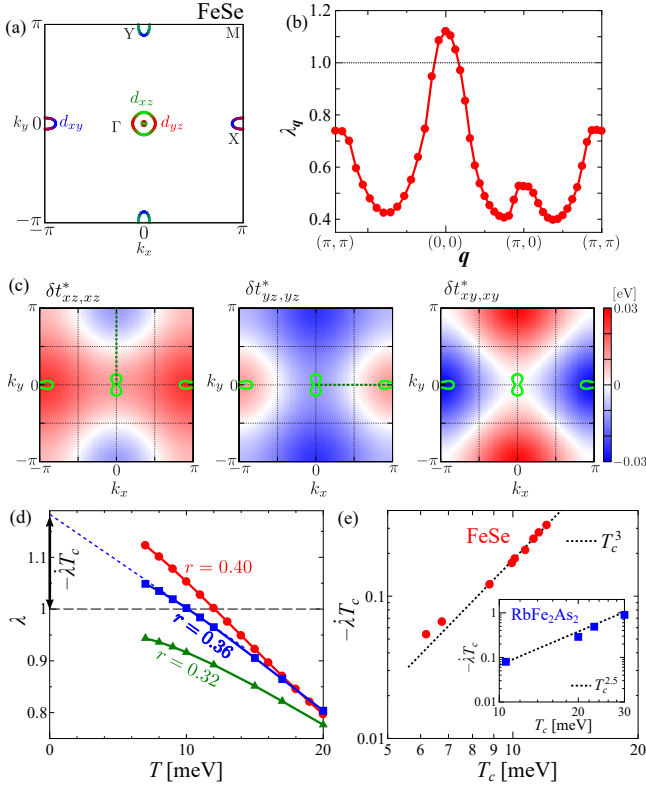


FIG. 4: (a) FS of FeSe model. Here, the weights of the xz , yz , and xy orbitals are shown by green, red, and blue colors. (b) Obtained eigenvalue $\lambda_{\mathbf{q}}$ at $T = 5\text{meV}$ and $r = 0.40$ derived from the linearized DW equation. The fact that $\lambda_{\mathbf{q}}$ exhibits the maximum at $\mathbf{q} = \mathbf{0}$ means the emergence of the ferro-DW order. (c) Renormalized form factor at $\mathbf{q} = \mathbf{0}$, $\delta t_{\mathbf{k},m,m}^*$ with $m = m' = xz, yz$ and xy , derived from the full DW equation at $T = 5\text{meV}$; see Fig. 5. The deformed FS in the nematic state is shown. (d) T -dependence of $\lambda_{\mathbf{q}=\mathbf{0}}(T)$ for $r = 0.32, 0.36$ and 0.40 . (e) Obtained $R = (-\lambda T_c)$ as a function of T_c for $r = 0.40 \sim 0.32$. The relation $R \propto T_c^b$ with $b \approx 3$ holds. The inset shows R in the RbFe₂As₂ model. Note that $R \approx 1$ ($b = 0$) in the BCS superconductivity.

nematic state ($T < T_c$) in FeSe based on the paramagnon interference mechanism.

Now, we explain the procedure of the numerical study in detail: The total self-energy is given in Eq. (15), where Σ^0 is the normal self-energy without any symmetry breaking given by Eq. (A2). Here, we calculate Σ^0 at each T by subtracting its static and Hermitian part, $\Sigma^{0,H}(\mathbf{k}) \equiv (\Sigma^0(\mathbf{k}, +i\delta) + \Sigma^0(\mathbf{k}, -i\delta))/2$, in order to fix the shape of the FS [70]. Next, we derive the symmetry breaking part δt self-consistently based on the following procedure: (a) We first calculate $S_{\mathbf{k}} \equiv \frac{T}{N} \sum_{\mathbf{q}} G_{\mathbf{k}+\mathbf{q}}[\Sigma] W_{\mathbf{q}}[\Sigma]$, where $G_{\mathbf{k}}[\Sigma]$ and $W_{\mathbf{q}}[\Sigma]$ are functions of the total self-energy. (b) Next, we derive δt as

$$\delta t_{\mathbf{k}} = (1 - P_0)S_{\mathbf{k}}, \quad (56)$$

where P_0 is the projection operator for the totally-symmetric (A_{1g}) channel. (c) The total self-energy is given as $\Sigma = \Sigma_0 + \delta t$. We repeat (a)-(c) till δt converges.

It is easy to show that the δt -linear term of $S_{\mathbf{k}}$ gives the right-hand side of the linearized DW equation (39) with the kernel function in Eq. (A3). Thus, the full-DW equation is equivalent to the linearized-DW equation when δt is very small.

Figure 5 (a) represents the obtained renormalized order parameter $\delta t_m^*(\mathbf{k}) = z_m \delta t_m(\mathbf{k})$ for $m = xz$ and $m = xy$ at Y-point. The obtained $T_c = 12\text{meV}$ completely coincides with that given by the linearized DW equation. The nematic order occurs as the second-order, and the averaged order parameter $\delta t_{\text{av}}^* \equiv (|\delta t_{xz}^*| + |\delta t_{xy}^*|)/2$ at Y-point is about $2T_c$ at $T = 5\text{meV}$. Thus, the present theory gives the ratio $\delta t_{\text{av}}^*/T_c \sim 2$, which is similar to the ratio $\Delta_0^*/T_c^{\text{SC}} \sim 2$ in the BCS theory. Thus, both the development of χ_{nem} above T_c and the nematic order parameter below T_c are well explained by the present theory.

The relation $2|\delta t_{xz}^*| \approx |\delta t_{xy}^*|$ in Fig. 5 (a) indicates that both the $(xz + yz)$ -orbitals and xy -orbital equally contribute to the nematic order. In Appendix D, we explain the relative phase between xz -orbital and xy -orbital form factors, $\delta t_{xz,xz}(0, \pi)\delta t_{xy,xy}(0, \pi) < 0$, on the basis of the Ginzburg-Landau analysis. This relation is significant for the Lifshitz transition below T_c as we will explain below.

Due to the nematic order parameter, the FS with C_4 -symmetry in Fig. 4 (a) is deformed to the C_2 -symmetry FS depicted in Fig. 5 (b) at $r = 0.40$ and $T = 5\text{meV}$. The corresponding band-dispersions in the normal state and that in the nematic state are shown in Figs. 5 (c) and (d), respectively. They are renormalized by the factor $z \sim 5$ for xy orbital and $z \sim 3$ for xz, yz orbitals. The original band-dispersion is shown in Fig. 10 in Appendix C. The hole-pocket is elongated along the k_y -axis due to the xz, yz -orbital polarization [3, 48, 68]. Interestingly, the electron-pocket around Y-point disappears in the nematic state due to the $d_{x^2-y^2}$ -wave form factor on the xy -orbital. This nematic Lifshitz transition has been confirmed by many angle-resolved photoemission spectroscopy (ARPES) studies [49, 50]. The relative phase between two form factors, $\delta t_{xz,xz}(0, \pi)\delta t_{xy,xy}(0, \pi) < 0$, originates from the kinetic energy gain due to the pseudogap formation by the Lifshitz transition.

In addition, in the nematic phase, the hole-pocket is elongated along the k_y -axis due to the xz, yz -orbital polarization with the sign-reversal in \mathbf{k} -space. This has been also confirmed by ARPES studies [48, 68]. Thus, experimental key findings in the nematic states are satisfactorily reproduced by the present ‘‘paramagnon interference mechanism’’ [2, 3, 42, 56].

C. Connection between above and below T_c

In the previous subsection, we derived the nematic self-energy $\Sigma \equiv \Sigma^0 + \delta t$ based on the full DW equation. The

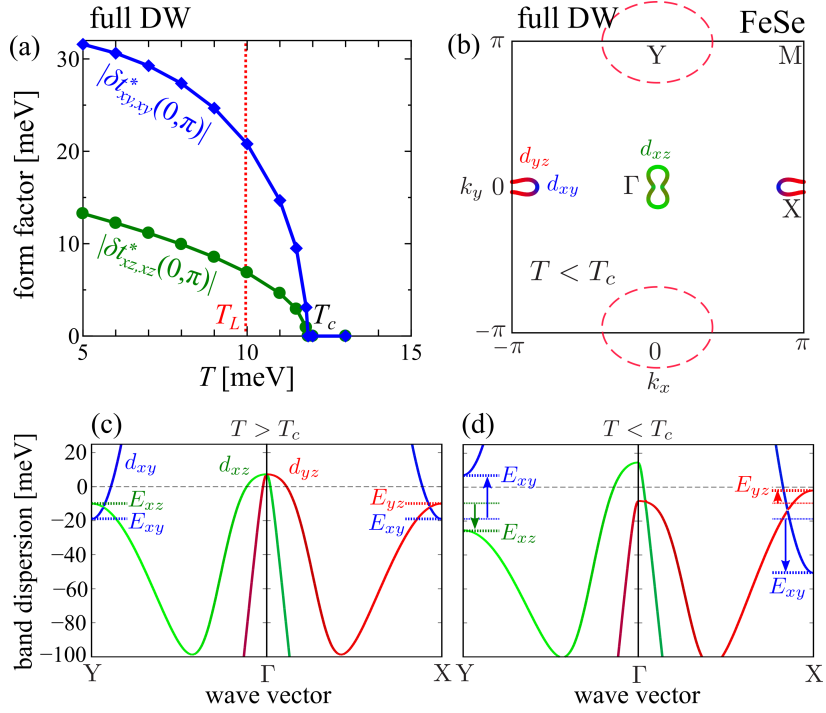


FIG. 5: (a) Obtained renormalized symmetry breaking self-energy $\delta t_{m,m}^*(\mathbf{k})$ for $m = xz, xy$ at Y-point, derived from the full DW equation at $r = 0.40$. The second-order transition occurs at $T_c = 12$ meV, which is consistent with the linearized DW equation analysis in Fig. 4 (d). T_L ($= 9$ meV) is the Lifshitz transition temperature. (b) FS in the nematic state at $T = 5$ meV ($< T_L$). The electron-pocket around Y-point disappears due to the xy -orbital form factor. In addition, the hole-pocket is elongated along the k_y -axis due to the xz, yz -orbital polarization with the sign-reversal in \mathbf{k} -space. (c) Renormalized band structure in the normal state. (d) Renormalized band structure in the nematic state.

derived nematic state corresponds to the stationary point of the LW grand potential $\Omega_{LW}[\Sigma]$, as proved in Sect. II. Because the obtained nematic state is thermodynamically stable, we can calculate the nematic susceptibility below T_c on the bases of the linearized DW equation with the nematic self-energy.

Figure 6 exhibits the eigenvalue of the linearized DW equation in the nematic state ($\Sigma \equiv \Sigma^0 + \delta t$), $\lambda_{\text{full-DW}}$, in the case of $r = 0.40$. (We also show the DW equation eigenvalue with the normal self-energy Σ^0 , $\lambda'(T)$, for reference.) We see that $\lambda(T)$ reaches unity at $T = T_c$, while it monotonically decreases for $T < T_c$. We find that $1 - \lambda(T) \approx |1 - \lambda'(T)|$ for $T \leq T_c$, as naturally expected in the GL theory. The beautiful numerical result in Fig. 6 means that the nematic-state derived from the full-DW method corresponds to the stationary point of Ω very accurately. Thus, electronic states of FeSe both above and below T_c are understood in a unified way based on the paramagnon interference mechanism.

The nematic susceptibility in the nematic state $T < T_c$ is $\chi_{\text{nem}}(T = 0) = \chi^{0f}(0)/(1 - \lambda(T = 0))$, where $1 - \lambda(T = 0) \approx R$. Since R ($\propto T_c^3$) is much smaller than unity as shown in Fig. 4 (e), the present study clarified that sizable nematic fluctuations remain in the nematic phase in Fe-based superconductors. This is an important information to understand the pairing mechanism in FeSe.

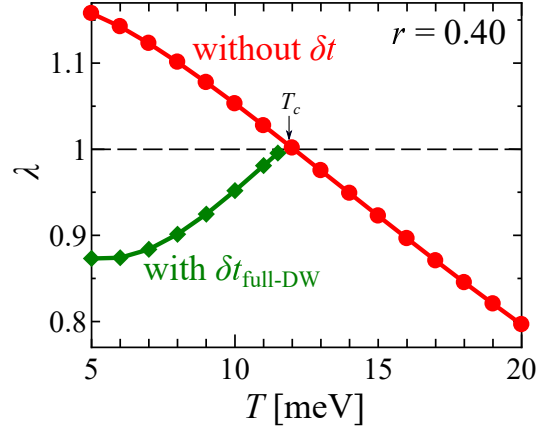


FIG. 6: Eigenvalue of the DW equation in the nematic state $\lambda(T)$ with the “nematic self-energy $\Sigma^0 + \delta t$ ”, where δt is derived from the full DW equation. Because $\Sigma^0 + \delta t$ represents the thermal equilibrium state, the nematic susceptibility $\bar{\chi}_{\text{nem}}(T) = (1 - \lambda(T))^{-1}$ is positive and diverges at $T = T_c$.

V. DISCUSSIONS

In this section, we discuss important unsolved properties in Fe-based SCs based on the present theory. We analyze the specific heat jump at $T = T_c$ in Sect. V A,

and calculate the T -dependence of χ_{nem} near the nematic QCP in Sect. VB.

A. Jump in the specific heat at T_c in FeSe

From the stationary point of the free energy ($\partial\Omega_{\text{DW}}(T, \mu, \phi)/\partial\phi|_{T, \mu} = 0$), we obtain $\phi = 0$ and $\phi = \sqrt{\frac{-a(T)}{b}}$ above and below T_c , respectively. Here, we assume a simple T -dependence of a , $a(T) = \dot{a}(T - T_c)$, where $\dot{a} = -\left.\frac{da}{dT}\right|_{T_c} (> 0)$. Then, we obtain the BCS-like order parameter for $T < T_c$ is

$$\phi = \sqrt{\frac{\dot{a}}{b}(T_c - T)}. \quad (57)$$

Then, the order parameter at $T = 0$ is $\phi_0 \approx \sqrt{(\dot{a}T_c)/b}$.

Based on the GL free energy, we discuss the jump of the heat capacity ΔC due to the DW transition, which is calculated by

$$\frac{\Delta C_{\text{DW}}}{T_c} = -\left.\frac{d^2\Omega_{\text{DW}}}{dT^2}\right|_{T=T_c} = (\dot{a}T_c) \left(\frac{\phi_0}{T_c}\right)^2. \quad (58)$$

Now, we calculate \dot{a} based on Eq. (50). In FeSe, $\chi^{0f}(0)$ is almost independent of T , while $-\dot{\lambda} \equiv -\left.\frac{d\lambda}{dT}\right|_{T_c}$ takes a large positive value as shown in Fig. 4 (d), due to the AL-type VCs in the kernel function I . Then, we obtain

$$(\dot{a}T_c) = 2\chi^{0f}(0)(-\dot{\lambda}T_c). \quad (59)$$

Note that $\chi^{0f}(0)$ is equal to the DOS projected by the form factor f , $D^f(0) \equiv \frac{1}{N} \sum_{\mathbf{k}} \delta(\epsilon_{\mathbf{k}} - \mu) f_{\mathbf{k}}^2$, in the absence of the self-energy.

Hereafter, we explicitly consider the mass-enhancement factor due to the self-energy, $z^{-1} \equiv 1 - \partial\text{Re}\Sigma/\partial\epsilon|_{\epsilon=\mu}$. The relation $z^{-1} \gg 1$ holds in general strongly correlated metals. In the Fermi liquid theory, the Green function is given as $G_{\mathbf{k}} = z/(i\epsilon_n - z(\epsilon_{\mathbf{k}} - \mu))$. Then, the DOS is changed to $\chi_z^{0f}(0) = z\chi_{z=1}^{0f}(0) = zD^f(0)$, and the observed renormalized order parameter is $\phi_0^* \equiv z\phi_0$. Thus, $\Delta C_{\text{DW}}/T_c$ due to the nematic transition is given by

$$\frac{\Delta C_{\text{DW}}}{T_c} = 2z^{-1}D^f(0)R \left(\frac{\phi_0^*}{T_c}\right)^2, \quad (60)$$

where $R = (-\dot{\lambda}T_c)$. As we summarized in Fig. 4 (e), $R \sim 0.3$ for $r = 0.40$, and $R \sim 0.1$ for $r = 0.36$. In contrast, $\Delta C_{\text{SC}}/T_c^{\text{SC}}$ due to the BCS superconductivity is $\Delta C_{\text{SC}}/T_c^{\text{SC}} = 2z^{-1}D^f(0) (\psi_0^*/T_c^{\text{SC}})^2$ with $\Delta = \psi \cdot f$, which corresponds to $R = 1$ in Eq. (60). ($\psi_0^* \equiv z\psi_0$ is the observed gap function.) Because $\psi_0^*/T_c^{\text{SC}} \approx 2$, we obtain $\Delta C_{\text{SC}}/T_c^{\text{SC}} = 8z^{-1}D^f(0)$, which is close to $9.4z^{-1}D^f(0)$ in the BCS theory. Because $\phi_0^*/T_c^{\text{SC}} \approx 2$ in the present numerical study, we obtain the relation

$$\frac{\Delta C_{\text{DW}}}{T_c} \sim R \frac{\Delta C_{\text{SC}}}{T_c^{\text{SC}}}. \quad (61)$$

In the present theory, $R \propto T_c^b$ with $b \sim 3$ for $r = 0.40 \sim 0.34$ ($T_c = 12 \sim 6\text{meV}$) as shown in Fig. 4 (e). Thus, the relation $\frac{\Delta C_{\text{DW}}}{T_c} \propto T_c^b$ is predicted by the present theory.

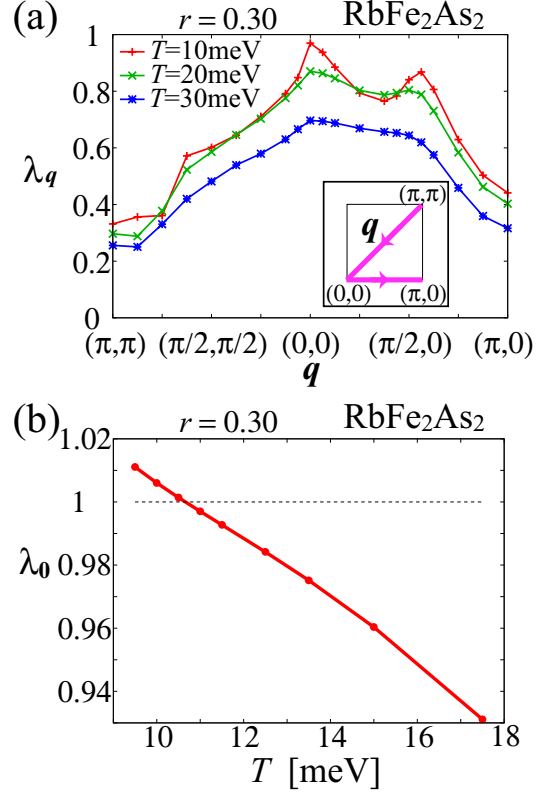


FIG. 7: (a) Obtained eigenvalue $\lambda_{\mathbf{q}}$ for RbFe₂As₂ model at $r = 0.30$ [69]. The obtained form factor at $\mathbf{q} = \mathbf{0}$ is the d_{xy} -symmetry bond order on xy -orbital. Here, we take the renormalization factor $z = 1/2$ into account by following Ref. [2]. (b) T -dependence of $\lambda_{\mathbf{q}=\mathbf{0}}$ in RbFe₂As₂ model.

Next, we discuss the nematic state in RbFe₂As₂, which is a heavily hole-doped Fe-based superconductor. This system exhibits the uniform ($\mathbf{q} = \mathbf{0}$) nematic order. Interestingly, the observed nematicity possesses the d_{xy} -wave symmetry, whose director is 45-degrees rotated from the $d_{x^2-y^2}$ -wave nematicity in FeSe. Figure 7 (a) shows the DW equation eigenvalue in the RbFe₂As₂ Hubbard model, which was introduced in Ref. [69]. The obtained form factor at $\mathbf{q} = \mathbf{0}$ is the d_{xy} -wave bond order on xy -orbital, as we revealed in Ref. [69]. Here, we set $\Sigma^0 = (1 - z^{-1})(i\epsilon_n - \mu)$ by following Ref. [2], instead of calculating the FLEX self-energy. We set the renormalization factor $z = 1/2$ ($= m/m^*$). Then, T_c is renormalized to be $T_c^* = zT_c$, and $\lambda_{\mathbf{q}}^{z=1}(T)$ is equal to $\lambda_{\mathbf{q}}^z(zT)$ [2].

Figure 7 (b) exhibits the T -dependence of $\lambda_{\mathbf{q}=\mathbf{0}}$. Here, the relations $R \sim 0.1$ when $T_c \sim 10\text{meV}$ and $R \propto T_c^b$ ($b \sim 2.5$) are obtained in the RbFe₂As₂ model. This result indicates that the relation $R \sim 0.01$ is satisfied at $T_c \sim 40\text{K}$. In fact, in FeSe model, we obtained the

relation $R \propto T_c^b$ ($b \sim 3$) at low T_c ($= 6 \sim 12\text{meV}$) by using fine \mathbf{k} -meshes (64^2) and many Matsubara frequencies (8192) to obtain reliable results at low T ; see Fig. 4 (e). Similar relation is expected to be realized in other Fe-based superconductor models within the same paramagnon interference mechanism. Therefore, the present theory gives a natural explanation why $\frac{\Delta C_{\text{DW}}}{T_c}$ in RbFe_2As_2 ($T_c \approx 40\text{K}$) reported in Ref. [53] is much smaller than that in FeSe ($T_c \approx 90\text{K}$) in Ref. [71].

B. CW/non-CW behavior in Nematic susceptibility

Here, we discuss the nematic susceptibility χ_{nem} due to the electron correlation. According to Ref. [67, 69], the nematic susceptibility is given as

$$\chi_{\text{nem}} = zD^f(0)\frac{1}{1-\lambda(T)}, \quad (62)$$

where $\lambda(T)$ is the eigenvalue of the DW equation with the “normal self-energy” Σ^0 . Figure 8 (a) shows the normalized susceptibility $\bar{\chi}_{\text{nem}} \equiv \chi_{\text{nem}}/\chi_{\text{nem}}^0 = 1/(1-\lambda(T))$ for $r = 0.40$ and 0.34 , which corresponds to $T_c = 12\text{meV}$ and 6.2meV respectively. In both cases, $\bar{\chi}_{\text{nem}}$ follows the CW behavior at higher temperatures ($T > T^* \sim 10\text{meV}$). In contrast, at lower temperatures ($T < T^*$) for $r = 0.34$, $\bar{\chi}_{\text{nem}}$ exhibits a clear deviation from the CW behavior. The Weiss temperature T_0 is derived from Fig. 8 (b): We see that $\lambda(T)$ changes from T -linear to T^2 -like at $T \sim T^* \sim 8\text{meV}$. Similar Fermi-liquid behavior in $\lambda(T)$ is also recognized in Fig. 4 (d). This result is natural because the system is far from the magnetic QCP. Thus, the present theory provides a natural explanation for the non-CW χ_{nem} near the nematic QCP with $T_c \approx 0$ reported in Refs. [12].

Here, we discuss the reason why χ_{nem} exhibits the CW/non-CW behavior depending on r . According to Eq. (40), the eigenvalue λ_q at $q = 0$ is proportional to X in Eq. (41) because $\chi^{0f}(q=0)$ is almost constant. In FeSe , the nematic state is mainly caused by the “paramagnon interference AL term” in X_q . It is approximately given as

$$X_{q=0} = T \sum_{Q,m} 3|\Lambda_{Q,q=0}^{f,m}|^2 (U^2 \chi_Q^{s,m})^2, \quad (63)$$

where $\chi_Q^{s,m}$ is the spin susceptibility for d -orbital m , and $\Lambda_{Q,q}^{f,m}$ is the three-point vertex composed of three Green functions:

$$\Lambda_{Q,q=0}^{f,m} = -T \sum_p \{ \hat{G}_p^0 \hat{f}_p^{q=0} \hat{G}_p^0 \}_{m,m} \{ \hat{G}_{p+Q}^0 \}_{m,m}, \quad (64)$$

where \hat{G}_p^0 is the matrix representation of the multi-orbital Green function with FLEX self-energy. Their expressions are shown in Fig. 8 (c). In a simple single-orbital model, the analytic expression of Eq. (64) is

$$\text{given as } \Lambda_{Q,q=0}^f = \frac{1}{N} \sum_{\mathbf{k}} \left(-\frac{\partial n(\epsilon_{\mathbf{k}})}{\partial \epsilon_{\mathbf{k}}} \right) \frac{1}{\epsilon_{\mathbf{k}-Q} - \epsilon_{\mathbf{k}}} f_{\mathbf{k}}^{q=0},$$

where $n(\epsilon)$ is the Fermi distribution function [72]. When $Q \approx Q_{\text{nesting}}$, $\Lambda_{Q,q=0}^f$ exhibits strong enhancement at low temperatures due to $(-\partial n(\epsilon_{\mathbf{k}})/\partial \epsilon_{\mathbf{k}})$ [2, 72].

In FeSe , the spin Stoner factor α_S is nearly constant for $T > T_c$. Then, the strong T -dependence of $\lambda(T)$ originates from $\Lambda_{Q,q=0}^f$, not from V_Q^s , as we explained in Ref. [2]. The paramagnon interference magnifies the nematic susceptibility, but its magnification is nearly constant. To confirm this fact, we introduce a simplification of $X_{q=0}$ in Eq. (63) as follows:

$$\bar{X}_{q=0} = T \sum_{Q,m} |\Lambda_{Q,q=0}^{f,m}|^2. \quad (65)$$

Figure 8 (d) shows the numerical result of $\bar{X}_{q=0}$ at $r = 0.34$. For $T \gtrsim 10\text{meV}$, $\bar{X}_{q=0}$ exhibit almost perfect T -linear behavior. Its increment at low T originates from the FS nesting. In contrast, at lower temperatures, $\bar{X}_{q=0}$ starts to saturate when T is smaller than the nesting energy scale [2]. This saturation gives rise to the non-CW behavior of χ_{nem} near the nematic QCP ($T_c \sim 0$) as shown in Fig. 8 (a).

Thus, the paramagnon interference mechanism satisfactorily explains both the CW behavior of χ_{nem} above T^* ($\sim 10\text{meV}$) and its non-CW behavior below T^* . These behaviors are actually observed in various Fe-based superconductors near the nematic QCP: $\text{Ba}(\text{Fe},\text{T})_2\text{As}_2$ with $\text{T}=\text{Co},\text{Ni}$, $(\text{Ba},\text{A})\text{Fe}_2\text{As}_2$ with $\text{A}=\text{K},\text{Rb}$, and $\text{Fe}(\text{Se},\text{Pn})$ with $\text{Pn}=\text{Te},\text{S}$ [14, 52, 54]. (In this mechanism, $\Lambda_{Q,q=0}^f$ is the coupling constant between the nematicity and the paramagnons, and its increment leads to large χ_{nem} at low temperatures.) Once the nematic order is established below T_c , the spin Stoner factor α_S increases as we discussed in [3, 73].

In the present mechanism, the deviation from the CW behavior of χ_{nem} below T^* is equal to the Fermi-liquid behavior $\lambda(0) - \lambda(T) \propto T^2$. This deviation is naturally expected when the nematic QCP is well separated from the magnetic QCP, even in the absence of impurities. We will discuss this point in the Summary section.

VI. SUMMARY

In this paper, we derived a formally exact “density-wave (DW) equation”, by introducing the form factor of the DW state $\delta t_{\mathbf{k}}^{q\sigma}$ into the LW theory. Its solution automatically satisfies the extremum condition of the grand potential. By solving the DW equation, the optimized form factor and its wavevector are uniquely obtained for both above and below T_c . This formalism enables us to perform the Baym-Kadanoff conserving approximation that is essential to obtain thermodynamic stable states. In addition, we derive an exact expression of the Ginzburg-Landau (GL) free energy, $F \propto a_q \phi^2$, where ϕ

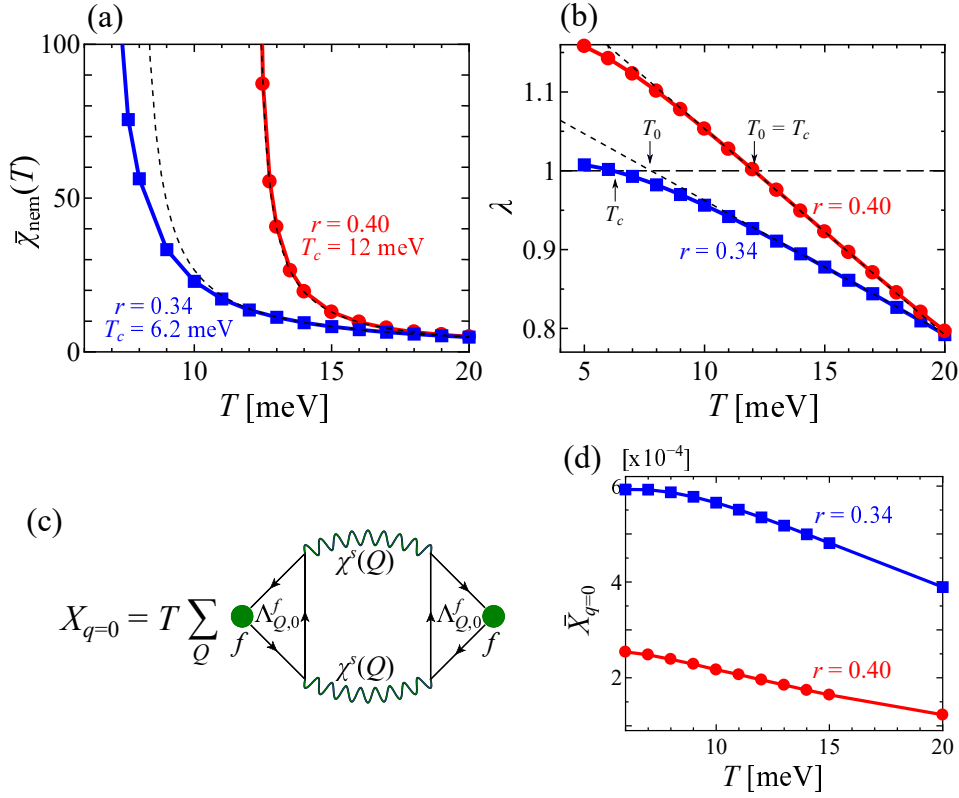


FIG. 8: (a) Nematic susceptibility $\bar{\chi}_{\text{nem}} = 1/(1 - \lambda(T))$ for $r = 0.34$ and 0.40 as a function of T . $\bar{\chi}_{\text{nem}}$ follows the CW behavior ($C/(T - T_0)$) at higher temperatures. However, it deviates from the CW behavior at low temperatures. (b) Derivation of the Weiss temperature T_0 from $\lambda(T)$. (c) The “paramagnon interference AL term” $X_{q=0}$ that is proportional to $\lambda_{q=0}$. $\Lambda_{q=0}^f(\mathbf{Q})$ is the three-point vertex. (d) Obtained $\bar{X}_{q=0}$ as a function of T . $\bar{X}_{q=0}$ starts to saturate at low temperatures, consistently with the deviation from the CW law in $\bar{\chi}_{\text{nem}}$.

is the amplitude of the DW order at wavevector \mathbf{q} . The coefficient $a_{\mathbf{q}} [\approx a_{\mathbf{q}_0} + \frac{1}{2} \sum_{\mu,\nu} c_{\mu,\nu} (q^\mu - q_0^\mu)(q^\nu - q_0^\nu)]$ is uniquely related to the eigenvalue of the DW equation $\lambda_{\mathbf{q}}$. This formalism enables us to calculate various thermodynamic properties of the DW state.

In the second part, we analyzed the nematic state in FeSe based on the derived DW equation based on a realistic multiorbital Hubbard model with one single parameter r . We explained the following key experiments in Fe-based SCs: **(i)** Lifshitz transition due to bond+orbital order [49, 50]. **(ii-1)** The CW behavior of $\chi_{\text{nem}} \propto 1/|1 - \lambda(T)|$ at higher-temperatures; $1 - \lambda(T) \propto T_0 - T$. **(ii-2)** Deviation from the CW behavior of χ_{nem} at low temperatures near the nematic QCP without magnetic criticality; $\lambda(0) - \lambda(T) \propto T^2$ [12, 13, 52]. **(iii)** A scaling relation $\Delta C/T_c \propto T_c^b$ ($b \sim 3$) that naturally explains the smallness of $\Delta C/T_c$ reported in several nematic systems [18, 19, 53]. This is because the gain of the free energy in the nematic transition is much smaller than that in the SC state. In addition, we explain the **(iv)** Nematic QCP away from the magnetic QCP observed in Fe(Se,S), Fe(Se,Te), [54] and Na(Fe,Co)As [55].

The present theory naturally explains the essential points **(i)-(iv)**. Thus, it is concluded that the nematic-

ity in FeSe is the bond+orbital order due to the “paramagnon interference mechanism” depicted in Fig. 8 (c) [2, 3, 42, 56].

The behavior **(ii-2)** has been observed in various Fe-based superconductors near the nematic QCP: Ba(Fe,T)₂As₂ with T=Co,Ni, (Ba,A)Fe₂As₂ with A=K,Rb, and Fe(Se,Pn) with Pn=Te,S [14, 54]. This behavior is frequently ascribed to the impurity-induced Griffiths phase, while it is widely observed insensitively to the impurity potential strength. (For example, the quantum oscillation is observed in Te- and S-doped FeSe.) In the present theory, the behavior **(ii-2)** is naturally explained when the nematic QCP is well separated from the magnetic QCP, even in the absence of impurities. It is useful to verify the relation $\lambda(0) - \lambda(T) \propto T^2$ experimentally. In the present mechanism, the increment of χ_{nem} at low T originates from the T -dependence of $\Lambda_{Q,q=0}$ in Eq. (64) [2], and the self-energy due to thermal spin fluctuations [66, 74] is also important to derive a perfect CW behavior of χ_{nem} . The self-energy due to nematic fluctuations will be also important ($|\Sigma_{\text{nem}}| \gtrsim |\Sigma_{\text{FLEX}}|$) adjacent to the nematic QCP, unless the dynamical nematic fluctuations are suppressed by the acoustic phonons. This is an important future issue. It is considered that a perfect

CW behavior for 30-250K observed in $\text{BaFe}_2(\text{As}_{0.3}\text{P}_{0.7})_2$ [14] is ascribed to the magnetic criticality due to the coincidence of the nematic and magnetic QCPs.

The present theory paves the way for understanding various unconventional phase transition systems for both above and below T_c . For example, the analysis of the odd-parity DW order accompanying spontaneous current, which has been reported in cuprates and kagome metals recently, is an important future problem [43, 59]. The (local and/or non-local) multipole order physics in $5d$ - and f -electron systems with strong spin-orbit interaction is another important future issue [31]. In addition, it is important to develop the numerical method beyond the one-loop approximation. the functional-renormalization-group method [42, 59, 75–77], which is equivalent to the parquet equation, would be useful to obtain a reliable kernel function of the DW equation. The exotic superconductivity mediated by the DW fluctuations [22, 78–80] would be a very interesting future problem.

Acknowledgments

We are grateful to E.-G. Moon for very enlightening discussions. We also thank Y. Matsuda, T. Shibauchi, T. Hashimoto, and Y. Mizukami for fruitful discussions on experiments. This work is supported by Grants-in-Aid for Scientific Research (KAKENI) Research (No. JP20K22328, No. JP20K03858, No. JP19H05825, No. JP18H01175) from MEXT of Japan.

Appendix A: Justification of Onari-Kontani approximation in the DW equation

Here, we derive the DW equation introduced by Onari and Kontani *et al.* in Refs. [3, 20, 21, 42], which has been applied to iron-based and cuprate superconductors, from the exact DW equation given in Eq. (36). In the present calculation, we apply the fluctuation-exchange (FLEX) approximation for $\Phi_{\text{FLEX}}[G]$. It is given as [62]

$$\begin{aligned} \Phi_{\text{FLEX}} &= T \sum_q \text{Tr} \left\{ \frac{3}{2} \ln(1 - U^s \chi_q^0) + \frac{1}{2} \ln(1 - U^c \chi_q^0) \right\} \\ &+ \frac{T}{4} \sum_q \text{Tr} \left\{ (U^s \chi_q^0)^2 + (U^c \chi_q^0)^2 \right\} \\ &+ T \sum_q \text{Tr} \left\{ \frac{3}{2} U^s \chi_q^0 + \frac{1}{2} U^c \chi_q^0 \right\}, \end{aligned} \quad (\text{A1})$$

which is expressed in Fig.9 (a). Here, $U^{s(c)}$ is the spin-channel (charge-channel) Coulomb interaction, and $U^s = -U^c = U$ in the single-orbital Hubbard model. Their matrix expressions in multiorbital systems are introduced in the next section.

In the framework of the conserving approximation, the first-order derivative of $\Phi_{\text{FLEX}}[G]$ gives the self-energy Σ .

It is expressed as [81, 82]

$$\Sigma_k^0 = \frac{T}{N} \sum_q G_{k+q}^0 W_q^0, \quad (\text{A2})$$

which is expressed in Fig.9 (b). Here, $W_q^0 = \left(\frac{3}{2} V_q^s + \frac{1}{2} V_q^c \right)$, $V_q^x = U^x + U^x \chi_q^x U^x$ ($x = s, c$), and $\chi_q^x = \chi^0(q)/(1 - U^x \chi^0(q))$.

Finally, we derive the irreducible four-point vertex I from the second derive of $\Phi_{\text{FLEX}}[G]$. The derived charge-channel kernel function in the DW equation (39) for $x = c$ is given by [20, 43]

$$\begin{aligned} I_{kk'q}^c &= -\frac{3}{2} V_{k-k'}^s - \frac{1}{2} V_{k-k'}^c \\ &+ \frac{T}{N} \sum_p \left[\frac{3}{2} V_{p+q}^s V_p^s + \frac{1}{2} V_{p+q}^c V_p^c \right] G_{k-p}^0 G_{k'-p}^0 \\ &+ \frac{T}{N} \sum_p \left[\frac{3}{2} V_{p+q}^s V_p^s + \frac{1}{2} V_{p+q}^c V_p^c \right] G_{k-p}^0 G_{k'+p}^0, \end{aligned} \quad (\text{A3})$$

which is depicted in Fig.9 (c). Note that the double-counting U^2 -terms in Eqs. (A3) and (A2) should be subtracted properly.

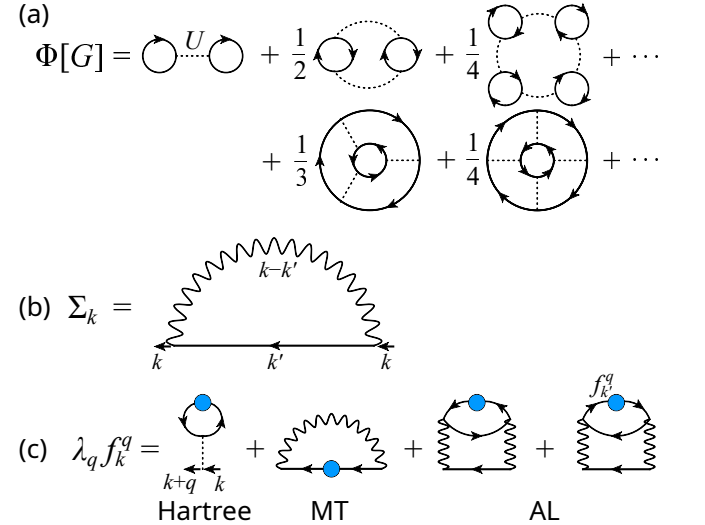


FIG. 9: (a) Diagrammatic expressions of $\Phi_{\text{FLEX}}[G]$ in the one-loop approximation. For simplicity, diagrams in the single-orbital Hubbard models are shown, while we study multi-orbital Hubbard models in this paper. (b) Self-energy $\Sigma_k = \delta \Phi_{\text{FLEX}} / \delta G_k$. (c) Linearized DW equation with the kernel function I derived from the second derivative of $\Phi_{\text{FLEX}}[G]$ with respect to G . The Maki-Thompson (MT) term and the Aslamazov-Larkin (AL) terms give the “fluctuation-induced interaction for the DW”.

Although the DW equation with the kernel in Eq. (A3) is an approximation, it satisfies the Baym-Kadanoff’s conserving laws by introducing Σ_{FLEX} . That is, the solution of the DW equation is the thermal equilibrium state derived from the stationary condition of Ω_{FLEX} . Thus,

the Onari-Kontani type DW equation [3, 20, 21, 42] is given by dropping Σ_{FLEX} from Eq. (A3). Furthermore, the present exact DW equation is useful to go beyond the Onari-Kontani's approximation.

Appendix B: GL free energy from $\Omega[G]$

In the main text, we derive the GL free energy based on the grand potential $\Omega[\Sigma]$. Here, we show a different way to obtain GL free energy by using $\Omega[G]$ starting from Eq. (14) in the main text. The coefficient a is derived from the second functional derivation of $\Omega[G]$ as

$$\Omega[\bar{G}] - \Omega[G^0] = \sum_{k\sigma k'\sigma'} \frac{\delta^2 \Omega[G]}{\delta G_{k'\sigma'} \delta G_{k\sigma}} \Big|_{G=G^0} \times \delta G_{k'\sigma'} \delta G_{k\sigma} \quad (\text{B1})$$

$$\begin{aligned} \frac{\delta^2 \Omega[G]}{\delta G_{k'\sigma'} \delta G_{k\sigma}} &= \frac{\delta}{\delta G_{k'\sigma'}} \{ G_{k\sigma}^{-1} - (G_{k\sigma}^{\text{free}})^{-1} + \Sigma_{k\sigma}[G] \} \\ &= -G_{k\sigma}^{-2} \delta_{kk'} - \frac{\delta \Sigma_{k\sigma}[G]}{\delta G_{k'\sigma'}} \\ \frac{\delta^2 \Omega[G]}{\delta G_{k\sigma} \delta G_{k'\sigma'}} \Big|_{G=G^0} &= -(G_{k\sigma}^0)^{-2} \delta_{kk'} - I_{kk'}^{\sigma\sigma'}. \end{aligned} \quad (\text{B2})$$

Thus, we obtain the following results

$$\begin{aligned} \Omega[G] - \Omega[G^0] &= \frac{T}{N} \sum_{k\sigma} (G_{k\sigma}^0)^{-2} (\delta G_{k\sigma})^2 \\ &\quad - \frac{T}{N} \sum_{k\sigma k'\sigma'} I_{kk'}^{\sigma\sigma'} \delta G_{k\sigma} \delta G_{k'\sigma'} \\ &= \chi^f(0) \{1 - \lambda\} \phi^2, \end{aligned} \quad (\text{B3})$$

where we use the relation $\delta G_{k\sigma} = (G_{k\sigma}^0)^2 \delta t_{k\sigma}$ and set $t_{k\sigma} = f_{k\sigma} \cdot \phi$. Therefore, the coefficient a of GL free energy from $\Omega[G]$ is given by

$$a = \chi^f(0) \{1 - \lambda\} \phi^2. \quad (\text{B4})$$

At $T = T_c$, the obtained a by $\Omega[G]$ is the same as the one by $\Omega[\Sigma]$ in the main text, while it becomes different at $T \neq T_c$. Moreover, the expression a by $\Omega[G]$ does not reproduce the results by mean-field approximation. Thus, the expression of Eq. (B4) is correct only at $T = T_c$

Appendix C: Eight-orbital models for FeSe

Here, we introduce the eight-orbital d - p models for FeSe. We first derived the first-principles tight-binding models using the WIEN2k and WANNIER90 codes. Crystal structure parameters of FeSe is given in Refs. [83]. By following Ref. [2], we introduce the k -dependent shifts for orbital l , δE_l , in order to obtain the experimentally observed FSs [49, 50]. In this paper, we introduce the intra-orbital hopping parameters into the first-principles FeSe model in order to shift the d_{xy} orbital

band ($d_{xz/yz}$ -orbital band) at (Γ, M, X) points by $(0, -0.35, +0.40)$ $[(-0.22, 0, +0.16)]$ in units of eV. Such level shifts are introduced by the additional intra-orbital [2]. The band-dispersion of the present FeSe model without self-energy is shown in Fig. 10. Its Fermi surface is given in Fig. 4 (a) in the main text.

In this multiorbital model, the matrix expression of the non-interacting Green function is given as

$$\hat{G}_k^{\text{free}} = ((\epsilon_n - \mu)\hat{1} + \hat{h}_k^0)^{-1}, \quad (\text{C1})$$

where $k \equiv (\mathbf{k}, \epsilon_n)$, and \hat{h}_k^0 is the matrix expression of the kinetic term, which is given by the Fourier transformation of the tight-binding model.

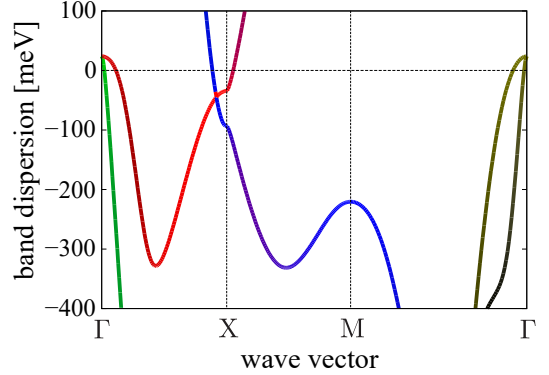


FIG. 10: Band-dispersion of the present FeSe model without self-energy. The renormalized dispersion due to the self-energy is shown in Fig. 5.

We also explain the multiorbital Coulomb interaction term H_U . The multiorbital Coulomb interaction term is expressed as $H_U = \frac{1}{4} \sum_{i,\sigma\sigma'} \sum_{l'l'mm'} U_{l'l'mm'}^{\sigma\sigma'} d_{i,l,\sigma}^\dagger d_{i,m',\sigma'}^\dagger d_{i,m,\sigma} d_{i,l',\sigma}$, where l, m represent the orbital indices, in $\sigma = +1$ (-1) represents the \uparrow (\downarrow) spin, i is the site index, and $\hat{U}^{\sigma\sigma'} = -\hat{U}^c - \sigma\sigma' \hat{U}^s$. The matrix elements of \hat{U}^s is given by [2]

$$(\hat{U}^s)_{l_1 l_2, l_3 l_4} = \begin{cases} U_{l_1, l_1}, & l_1 = l_2 = l_3 = l_4 \\ U'_{l_1, l_2}, & l_1 = l_3 \neq l_2 = l_4 \\ J_{l_1, l_3}, & l_1 = l_2 \neq l_3 = l_4 \\ J_{l_1, l_2}, & l_1 = l_4 \neq l_2 = l_3 \\ 0, & \text{otherwise.} \end{cases} \quad (\text{C2})$$

Also, the bare Coulomb interaction for the charge channel is

$$(\hat{U}^c)_{l_1 l_2, l_3 l_4} = \begin{cases} -U_{l_1, l_1}, & l_1 = l_2 = l_3 = l_4 \\ U'_{l_1, l_2} - 2J_{l_1, l_2}, & l_1 = l_3 \neq l_2 = l_4 \\ -2U'_{l_1, l_3} + J_{l_1, l_3}, & l_1 = l_2 \neq l_3 = l_4 \\ -J_{l_1, l_2}, & l_1 = l_4 \neq l_2 = l_3 \\ 0, & \text{otherwise.} \end{cases} \quad (\text{C3})$$

Here, $U_{l,l}$, $U'_{l,l'}$ and $J_{l,l'}$ are the first-principles Coulomb interaction terms given in Ref. [63].

In the main text, we omit the orbital indices of the Green functions and the Coulomb interactions to simplify the expressions. It is straightforward to write the orbital indices of these expressions in multiorbital models by using Eqs. (C1)-(C3).

Appendix D: Relative phase between xz -orbital and xy -orbital form factors

As we discussed in the main text, the relation $2|\delta t_{xz}^*| \approx |\delta t_{xy}^*|$ in Fig. 5 (a) indicates that both the $(xz + yz)$ -orbitals and xy -orbital equally contribute to the nematic order in FeSe. The $(xz + yz)$ -orbital polarization [xy -orbital bond order] originates from the spin fluctuations on $(xz + yz)$ -orbitals [xy -orbital]. Here, we discuss the relative phase between xz -orbital and xy -orbital form

factors, $\delta t_{xz,xz}(0, \pi) \times \delta t_{xy,xy}(0, \pi) < 0$, based on the Ginzburg-Landau analysis.

According to Eq. (48) or (49), the second-order inter-orbital free-energy is $F_{2,4}^{(2)} = -2\chi_{2,4}^{0f}\phi_2\phi_4$, where $\chi_{2,4}^{0\delta t} = -T\sum_k G_{2,4}(k)G_{4,2}(k)f_{2,2}(k)f_{4,4}(k)$ and $\delta t_{m,m}(k) = f_{m,m}(k)\phi_m$. We verified numerically that $\chi_{2,4}^{0f} > 0$, which is consistent with the relations $\chi_{22,44}^0(0) < 0$ in FeSe and $\delta t_{2,2}(k)\delta t_{4,4}(k) < 0$ around Y-point shown in Fig. 4 (c). Thus, the relation $\phi_2\phi_4 > 0$ is realized, and therefore the Lifshitz transition occurs in FeSe. In other words, the relation $\phi_2\phi_4 > 0$ (i.e., $\delta t_{2,2}(0, \pi)\delta t_{4,4}(0, \pi) < 0$) is a direct consequence of the multiorbital band structure of Fe-based superconductors.

-
- [1] A. V. Chubukov, M. Khodas, and R. M. Fernandes, *Magnetism, Superconductivity, and Spontaneous Orbital Order in Iron-Based Superconductors: Which Comes First and Why?*, Phys. Rev. X **6**, 041045 (2016).
- [2] Y. Yamakawa, S. Onari, and H. Kontani, *Nematicity and Magnetism in FeSe and Other Families of Fe-Based Superconductors*, Phys. Rev. X **6**, 021032 (2016).
- [3] S. Onari, Y. Yamakawa, and H. Kontani, *Sign-Reversing Orbital Polarization in the Nematic Phase of FeSe due to the C_2 Symmetry Breaking in the Self-Energy*, Phys. Rev. Lett. **116**, 227001 (2016).
- [4] R. M. Fernandes, A. V. Chubukov, and J. Schmalian, *What drives nematic order in iron-based superconductors?*, Nat. Phys. **10**, 97–104 (2014).
- [5] M. Yoshizawa, D. Kimura, T. Chiba, S. Simayi, Y. Nakanishi, K. Kihou, C.-H. Lee, A. Iyo, H. Eisaki, M. Nakaajima, and S.-i. Uchida, *Structural Quantum Criticality and Superconductivity in Iron-Based Superconductor $Ba(Fe_{1-x}Co_x)_2As_2$* , J. Phys. Soc. Jpn. **81**, 024604 (2012).
- [6] R. M. Fernandes, L. H. VanBebber, S. Bhattacharya, P. Chandra, V. Keppens, D. Mandrus, M. A. McGuire, B. C. Sales, A. S. Sefat, and J. Schmalian, *Effects of Nematic Fluctuations on the Elastic Properties of Iron Arsenide Superconductors*, Phys. Rev. Lett. **105**, 157003 (2010).
- [7] A. E. Böhmer, P. Burger, F. Hardy, T. Wolf, P. Schweiss, R. Fromknecht, M. Reinecker, W. Schranz, and C. Meingast, *Nematic Susceptibility of Hole-Doped and Electron-Doped $BaFe_2As_2$ Iron-Based Superconductors from Shear Modulus Measurements*, Phys. Rev. Lett. **112**, 047001 (2014).
- [8] Y. Gallais, R. M. Fernandes, I. Paul, L. Chauvière, Y.-X. Yang, M.-A. Méasson, M. Cazayous, A. Sacuto, D. Colson, and A. Forget, *Observation of Incipient Charge Nematicity in $Ba(Fe_{1-x}Co_x)_2As_2$* , Phys. Rev. Lett. **111**, 267001 (2013).
- [9] P. Massat, D. Farina, I. Paul, S. Karlsson, P. Strobel, P. Toulemonde, M.-A. Méasson, M. Cazayous, A. Sacuto, S. Kasahara, T. Shibauchi, Y. Matsuda, and Y. Gallais, *Charge-induced nematicity in FeSe*, Proc. Natl. Acad. Sci. U.S.A. **113**, 9177 (2016).
- [10] T. Kissikov, R. Sarkar, M. Lawson, B. T. Bush, E. I. Timmons, M. A. Tanatar, R. Prozorov, S. L. Bud'ko, P. C. Canfield, R. M. Fernandes, and N. J. Curro, *Uniaxial strain control of spin-polarization in multicomponent nematic order of $BaFe_2As_2$* , Nat. Commun. **9**, 1058 (2018).
- [11] I. R. Fisher, L. Degiorgi, and Z. X. Shen, *In-plane electronic anisotropy of underdoped '122' Fe-arsenide superconductors revealed by measurements of detwinned single crystals*, Rep. Prog. Phys. **74**, 124506 (2011).
- [12] S. Hosoi, K. Matsuura, K. Ishida, H. Wang, Y. Mizukami, T. Watashige, S. Kasahara, Y. Matsuda, and T. Shibauchi, *Nematic quantum critical point without magnetism in $FeSe_{1-x}S_x$ superconductors*, Proc. Natl. Acad. Sci. U.S.A. **113**, 8139 (2016).
- [13] K. Ishida, M. Tsujii, S. Hosoi, Y. Mizukami, S. Ishida, A. Iyo, H. Eisaki, T. Wolf, K. Grube, H. v. Löhneysen, R. M. Fernandes, and T. Shibauchi, *Novel electronic nematicity in heavily hole-doped iron pnictide superconductors*, Proc. Natl. Acad. Sci. U.S.A. **117**, 6424 (2020).
- [14] H.-H. Kuo, J.-H. Chu, J. C. Palmstrom, S. A. Kivelson, and I. R. Fisher, *Ubiquitous signatures of nematic quantum criticality in optimally doped Fe-based superconductors*, Science **352**, 958 (2016).
- [15] R. M. Fernandes and J. W. F. Venderbos, *Nematicity with a twist: Rotational symmetry breaking in a moiré superlattice*, Sci. Adv. **6**, eaba8834 (2020).
- [16] S. Onari and H. Kontani, *$SU(4)$ Valley+Spin Fluctuation Interference Mechanism for Nematic Order in Magic-Angle Twisted Bilayer Graphene: The Impact of Vertex Corrections*, Phys. Rev. Lett. **128**, 066401 (2022).
- [17] H. Nakaoka, Y. Yamakawa, and H. Kontani, *Theoretical prediction of nematic orbital-ordered state in the Ti oxypnictide superconductor $BaTi_2(As,Sb)_2O$* , Phys. Rev. B **93**, 245122 (2016).
- [18] Y. Sato, S. Kasahara, H. Murayama, Y. Kasahara, E.-G. Moon, T. Nishizaki, T. Loew, J. Porras, B. Keimer, T. Shibauchi, and Y. Matsuda, *Thermodynamic evidence for a nematic phase transition at the onset of the pseudogap in $YBa_2Cu_3O_y$* , Nat. Phys. **13**, 1074–1078 (2017).
- [19] H. Murayama, Y. Sato, R. Kurihara, S. Kasahara, Y.

- Mizukami, Y. Kasahara, H. Uchiyama, A. Yamamoto, E.-G. Moon, J. Cai, J. Freyermuth, M. Greven, T. Shibauchi, and Y. Matsuda, *Diagonal nematicity in the pseudogap phase of $HgBa_2CuO_4+\delta$* , Nat. Commun. **10**, 3282 (2019).
- [20] K. Kawaguchi, Y. Yamakawa, M. Tsuchiizu, and H. Kontani, *Competing Unconventional Charge-Density-Wave States in Cuprate Superconductors: Spin-Fluctuation-Driven Mechanism*, J. Phys. Soc. Jpn. **86**, 063707 (2017).
- [21] M. Tsuchiizu, K. Kawaguchi, Y. Yamakawa, and H. Kontani, *Multistage electronic nematic transitions in cuprate superconductors: A functional-renormalization-group analysis*, Phys. Rev. B **97**, 165131 (2018).
- [22] R. Tazai, Y. Yamakawa, S. Onari, and H. Kontani, *Mechanism of exotic density-wave and beyond-Migdal unconventional superconductivity in kagome metal AV_3Sb_5 ($A = K, Rb, Cs$)*, Sci. Adv. **8**, eabl4108 (2022).
- [23] M. L. Kiesel, C. Platt, and R. Thomale, *Unconventional Fermi Surface Instabilities in the Kagome Hubbard Model*, Phys. Rev. Lett. **110**, 126405 (2013).
- [24] W.-S. Wang, Z.-Z. Li, Y.-Y. Xiang, and Q.-H. Wang, *Competing electronic orders on kagome lattices at van Hove filling*, Phys. Rev. B **87**, 115135 (2013).
- [25] T. Park, M. Ye, and L. Balents, *Electronic instabilities of kagome metals: Saddle points and Landau theory*, Phys. Rev. B **104**, 035142 (2021).
- [26] Y. Yamakawa and H. Kontani, *Spin-Fluctuation-Driven Nematic Charge-Density Wave in Cuprate Superconductors: Impact of Aslamazov-Larkin Vertex Corrections*, Phys. Rev. Lett. **114**, 257001 (2015).
- [27] S. Sachdev and R. La Placa, *Bond Order in Two-Dimensional Metals with Antiferromagnetic Exchange Interactions*, Phys. Rev. Lett. **111**, 027202 (2013).
- [28] C. Husemann and W. Metzner, *Incommensurate nematic fluctuations in the two-dimensional Hubbard model*, Phys. Rev. B **86**, 085113 (2012).
- [29] C. Fang, H. Yao, W.-F. Tsai, J. Hu, and S. A. Kivelson, *Theory of electron nematic order in $LaFeAsO$* , Phys. Rev. B **77**, 224509 (2008).
- [30] F. Wang, S. A. Kivelson, and D.-H. Lee, *Nematicity and quantum paramagnetism in $FeSe$* , Nat. Phys. **11**, 959–963 (2015).
- [31] R. Tazai and H. Kontani, *Multipole fluctuation theory for heavy fermion systems: Application to multipole orders in CeB_6* , Phys. Rev. B **100**, 241103(R) (2019).
- [32] R. Tazai and H. Kontani, *Fully gapped s -wave superconductivity enhanced by magnetic criticality in heavy-fermion systems*, Phys. Rev. B **98**, 205107 (2018).
- [33] R. Tazai and H. Kontani, *Hexadecapole Fluctuation Mechanism for s -wave Heavy Fermion Superconductor $CeCu_2Si_2$: Interplay between Intra- and Inter-Orbital Cooper Pairs*, J. Phys. Soc. Jpn. **88**, 063701 (2019).
- [34] C. Mielke, D. Das, J.-X. Yin, H. Liu, R. Gupta, Y.-X. Jiang, M. Medarde, X. Wu, H. C. Lei, J. Chang, P. Dai, Q. Si, H. Miao, R. Thomale, T. Neupert, Y. Shi, R. Khasanov, M. Z. Hasan, H. Luetkens, and Z. Guguchia, *Time-reversal symmetry-breaking charge order in a kagome superconductor*, Nature **602**, 245–250 (2022).
- [35] Q. Wu, Z. X. Wang, Q. M. Liu, R. S. Li, S. X. Xu, Q. W. Yin, C. S. Gong, Z. J. Tu, H. C. Lei, T. Dong, and N. L. Wang, *Revealing the immediate formation of two-fold rotation symmetry in charge-density-wave state of Kagome superconductor CsV_3Sb_5 by optical polarization rotation measurement*, arXiv:2110.11306.
- [36] H. Murayama, K. Ishida, R. Kurihara, T. Ono, Y. Sato, Y. Kasahara, H. Watanabe, Y. Yanase, G. Cao, Y. Mizukami, T. Shibauchi, Y. Matsuda, and S. Kasahara, *Bond Directional Anapole Order in a Spin-Orbit Coupled Mott Insulator $Sr_2(Ir_{1-x}Rh_x)O_4$* , Phys. Rev. X **11**, 011021 (2021).
- [37] M. E. Simon and C. M. Varma, *Detection and Implications of a Time-Reversal Breaking State in Underdoped Cuprates*, Phys. Rev. Lett. **89**, 247003 (2002).
- [38] A. A. Nersesyan, G. I. Japaridze, and I. G. Kimeridze, *Low-temperature magnetic properties of a two-dimensional spin nematic state*, J. Phys.: Condens. Matter **3**, 3353 (1991).
- [39] E. Berg, E. Fradkin, S. A. Kivelson, and J. M. Tranquada, *Striped superconductors: how spin, charge and superconducting orders intertwine in the cuprates*, New J. Phys. **11**, 115004 (2009).
- [40] C. J. Halboth and W. Metzner, *Renormalization-group analysis of the two-dimensional Hubbard model*, Phys. Rev. B **61**, 7364 (2000).
- [41] J. C. S. Davis and D.-H. Lee, *Concepts relating magnetic interactions, intertwined electronic orders, and strongly correlated superconductivity*, Proc. Natl. Acad. Sci. U.S.A. **110**, 17623 (2013).
- [42] R. Tazai, Y. Yamakawa, M. Tsuchiizu, and H. Kontani, *d - and p -wave Quantum Liquid Crystal Orders in Cuprate Superconductors, κ -(BEDT-TTF) $_2X$, and Coupled Chain Hubbard Models: Functional-renormalization-group Analysis*, J. Phys. Soc. Jpn. **90**, 111012 (2021).
- [43] H. Kontani, Y. Yamakawa, R. Tazai, and S. Onari, *Odd-parity spin-loop-current order mediated by transverse spin fluctuations in cuprates and related electron systems*, Phys. Rev. Research **3**, 013127 (2021).
- [44] A. A. Abrikosov, L. P. Gorkov, and I. E. Dzyaloshinski, *Methods of Quantum Field Theory in Statistical Physics*, (New York: Dover Publications, Inc., 1975.)
- [45] J. M. Luttinger and J. C. Ward, *Ground-State Energy of a Many-Fermion System. II*, Phys. Rev. **118**, 1417 (1960).
- [46] G. Baym and L. P. Kadanoff, *Conservation Laws and Correlation Functions*, Phys. Rev. **124**, 287 (1961).
- [47] G. Baym, *Self-Consistent Approximations in Many-Body Systems*, Phys. Rev. **127**, 1391 (1962).
- [48] Y. Suzuki, T. Shimojima, T. Sonobe, A. Nakamura, M. Sakano, H. Tsuji, J. Omachi, K. Yoshioka, M. Kuwata-Gonokami, T. Watashige, R. Kobayashi, S. Kasahara, T. Shibauchi, Y. Matsuda, Y. Yamakawa, H. Kontani, and K. Ishizaka, *Momentum-dependent sign inversion of orbital order in superconducting $FeSe$* , Phys. Rev. B **92**, 205117 (2015).
- [49] M. Yi, H. Pfau, Y. Zhang, Y. He, H. Wu, T. Chen, Z. R. Ye, M. Hashimoto, R. Yu, Q. Si, D.-H. Lee, P. Dai, Z.-X. Shen, D. H. Lu, and R. J. Birgeneau, *Nematic Energy Scale and the Missing Electron Pocket in $FeSe$* , Phys. Rev. X **9**, 041049 (2019).
- [50] S. S. Huh, J. J. Seo, B. S. Kim, S. H. Cho, J. K. Jung, S. Kim, C. I. Kwon, J. S. Kim, Y. Y. Koh, W. S. Kyung, J. D. Denlinger, Y. H. Kim, B. N. Chae, N. D. Kim, Y. K. Kim, and C. Kim, *Absence of Y -pocket in 1- Fe Brillouin zone and reversed orbital occupation imbalance in $FeSe$* , Commun. Phys. **3**, 52 (2020).
- [51] L. C. Rhodes, J. Böker, M. A. Müller, M. Eschrig, and I. M. Eremin, *Non-local dxy nematicity and the miss-*

- ing electron pocket in FeSe, npj Quantum Mater. **6**, 45 (2021).
- [52] T. Terashima, Y. Matsushita, H. Yamase, N. Kikugawa, H. Abe, M. Imai, S. Uji, S. Ishida, H. Eisaki, A. Iyo, K. Kihou, C.-H. Lee, T. Wang, and G. Mu, *Elastoresistance measurements on CaKFe₄As₄ and KCa₂Fe₄As₄F₂ with the Fe site of C_{2v} symmetry*, Phys. Rev. B **102**, 054511 (2020).
- [53] Y. Mizukami, O. Tanaka, K. Ishida, M. Tsujii, T. Mitsui, S. Kitao, M. Kurokuzu, M. Seto, S. Ishida, A. Iyo, H. Eisaki, K. Hashimoto, and T. Shibauchi, *Thermodynamic Signatures of Diagonal Nematicity in RbFe₂As₂ Superconductor*, arXiv:2108.13081.
- [54] K. Ishida, Y. Onishi, M. Tsujii, K. Mukasa, M. Qiu, M. Saito, Y. Sugimura, K. Matsuura, Y. Mizukami, K. Hashimoto, and T. Shibauchi, *Pure nematic quantum critical point accompanied by a superconducting dome*, arXiv:2202.11674.
- [55] C. G. Wang, Z. Li, J. Yang, L. Y. Xing, G. Y. Dai, X. C. Wang, C. Q. Jin, R. Zhou, and G.-q. Zheng, *Electron Mass Enhancement near a Nematic Quantum Critical Point in NaFe_{1-x}Co_xAs*, Phys. Rev. Lett. **121**, 167004 (2018).
- [56] S. Onari and H. Kontani, *Self-consistent Vertex Correction Analysis for Iron-based Superconductors: Mechanism of Coulomb Interaction-Driven Orbital Fluctuations*, Phys. Rev. Lett. **109**, 137001 (2012).
- [57] H. J. Schulz, *Fermi-surface instabilities of a generalized two-dimensional Hubbard model*, Phys. Rev. B **39**, 2940(R) (1989).
- [58] I. Affleck and J. B. Marston, *Large-n limit of the Heisenberg-Hubbard model: Implications for high-T_c superconductors*, Phys. Rev. B **37**, 3774(R) (1988).
- [59] R. Tazai, Y. Yamakawa, and H. Kontani, *Emergence of charge loop current in the geometrically frustrated Hubbard model: A functional renormalization group study*, Phys. Rev. B **103**, L161112 (2021).
- [60] E. P. Wohlfarth, *Thermodynamic aspects of itinerant electron magnetism*, Physica B+C **91**, 305 (1977).
- [61] M. Potthoff, *Self-energy-functional approach to systems of correlated electrons*, Eur. Phys. J. B **32**, 429 (2003).
- [62] Y. Yanase and M. Ogata, *Kinetic Energy, Condensation Energy, Optical Sum Rule and Pairing Mechanism in High-T_c Cuprates*, J. Phys. Soc. Jpn. **74**, 1534 (2005).
- [63] T. Miyake, K. Nakamura, R. Arita, and M. Imada, *Comparison of Abinitio Low-Energy Models for LaFePO, LaFeAsO, BaFe₂As₂, LiFeAs, FeSe, and FeTe: Electron Correlation and Covalency*, J. Phys. Soc. Jpn. **79**, 044705 (2010).
- [64] H. Kontani and M. Ohno, *Effect of a nonmagnetic impurity in a nearly antiferromagnetic Fermi liquid: Magnetic correlations and transport phenomena*, Phys. Rev. B **74**, 014406 (2006).
- [65] R.-Q. Xing, L. Classen, and A. V. Chubukov, *Orbital order in FeSe: The case for vertex renormalization*, Phys. Rev. B **98**, 041108 (2018).
- [66] H. Kontani, *Anomalous transport phenomena in Fermi liquids with strong magnetic fluctuations*, Rep. Prog. Phys. **71**, 026501 (2008).
- [67] S. Onari and H. Kontani, *Hidden antiferronematic order in Fe-based superconductor BaFe₂As₂ and NaFeAs above T_S*, Phys. Rev. Research **2**, 042005(R) (2020).
- [68] Y. Zhang, M. Yi, Z.-K. Liu, W. Li, J. J. Lee, R. G. Moore, M. Hashimoto, M. Nakajima, H. Eisaki, S.-K. Mo, Z. Hussain, T. P. Devereaux, Z.-X. Shen, and D. H. Lu, *Distinctive orbital anisotropy observed in the nematic state of a FeSe thin film*, Phys. Rev. B **94**, 115153 (2016).
- [69] S. Onari and H. Kontani, *Origin of diverse nematic orders in Fe-based superconductors: 45° rotated nematicity in AFe₂As₂ (A = Cs, Rb)*, Phys. Rev. B **100**, 020507(R) (2019).
- [70] S. Onari and H. Kontani, *Iron-Based Superconductivity*, (ed. P.D. Johnson, G. Xu, and W.-G. Yin, Springer-Verlag Berlin and Heidelberg GmbH & Co. K (2015)).
- [71] A. E. Böhmer, T. Arai, F. Hardy, T. Hattori, T. Iye, T. Wolf, H. v. Löhneysen, K. Ishida, and C. Meingast, *Origin of the Tetragonal-to-Orthorhombic Phase Transition in FeSe: A Combined Thermodynamic and NMR Study of Nematicity*, Phys. Rev. Lett. **114**, 027001 (2015).
- [72] H. Kontani and Y. Yamakawa, *Linear Response Theory for Shear Modulus C₆₆ and Raman Quadrupole Susceptibility: Evidence for Nematic Orbital Fluctuations in Fe-based Superconductors*, Phys. Rev. Lett. **113**, 047001 (2014).
- [73] H. Kontani, T. Saito, and S. Onari, *Origin of orthorhombic transition, magnetic transition, and shear-modulus softening in iron pnictide superconductors: Analysis based on the orbital fluctuations theory*, Phys. Rev. B **84**, 024528 (2011).
- [74] S. Onari and H. Kontani, *In-plane anisotropy of transport coefficients in electronic nematic states: Universal origin of nematicity in Fe-based superconductors*, Phys. Rev. B **96**, 094527 (2017).
- [75] W. Metzner, M. Salmhofer, C. Honerkamp, V. Meden, and K. Schönhammer, *Functional renormalization group approach to correlated fermion systems*, Rev. Mod. Phys. **84**, 299 (2012).
- [76] M. Salmhofer and C. Honerkamp, *Fermionic Renormalization Group Flows: Technique and Theory*, Prog. Theor. Phys. **105**, 1 (2001).
- [77] M. Tsuchiizu, Y. Ohno, S. Onari, and H. Kontani, *Orbital Nematic Instability in the Two-Orbital Hubbard Model: Renormalization-Group + Constrained RPA Analysis*, Phys. Rev. Lett. **111**, 057003 (2013).
- [78] H. Kontani and S. Onari, *Orbital-Fluctuation-Mediated Superconductivity in Iron Pnictides: Analysis of the Five-Orbital Hubbard-Holstein Model*, Phys. Rev. Lett. **104**, 157001 (2010).
- [79] Y. Yamakawa and H. Kontani, *Nematicity, magnetism, and superconductivity in FeSe under pressure: Unified explanation based on the self-consistent vertex correction theory*, Phys. Rev. B **96**, 144509 (2017).
- [80] Y. Yamakawa and H. Kontani, *Superconductivity without a hole pocket in electron-doped FeSe: Analysis beyond the Migdal-Eliashberg formalism*, Phys. Rev. B **96**, 045130 (2017).
- [81] N. E. Bickers, D. J. Scalapino, and S. R. White, *Conserving Approximations for Strongly Correlated Electron Systems: Bethe-Salpeter Equation and Dynamics for the Two-Dimensional Hubbard Model*, Phys. Rev. Lett. **62**, 961 (1989).
- [82] S. Onari, Y. Yamakawa, and H. Kontani, *High-T_c Superconductivity near the Anion Height Instability in Fe-Based Superconductors: Analysis of LaFeAsO_{1-x}H_x*, Phys. Rev. Lett. **112**, 187001 (2014).
- [83] A. E. Böhmer, F. Hardy, F. Eilers, D. Ernst, P. Adelman, P. Schweiss, T. Wolf, and C. Meingast, *Lack of coupling between superconductivity and orthorhombic dis-*

tortion in stoichiometric single-crystalline FeSe, Phys. Rev. B **87**, 180505(R) (2013).